Response to Reviewer comment #1:

General comments:

The paper by Yang et al. presents results from a measurement campaign in September / October 2018 at Shenzhen in the Pearl River Delta. Unfortunately, the collected data-set is not state-of-the art and the subsequent interpretation suffers from this lack of data and thus the manuscript does not bring any useful new insight into atmospheric chemistry. The shortcomings in the data-set compared with what is current state-of-the art are:

Reply

Thanks for your helpful comments which would help us to improve the manuscript. The comments and suggestions are valuable and very helpful for us. We have taken all these suggestions into account and have made corrections in this revised manuscript. Below are our responses to the specific comments, highlighted in blue, with changes to the manuscript highlighted in green.

Specific comments:

1. OH reactivity has not been measured: the analysis of the radicals budget is based on calculated OH reactivity, which is unsatisfactorily, especially given that k_{OH} measurements are now widely available and add much confidence to the data set. Missing OH reactivity is widely observed under various conditions, and field campaigns quantifying OH and HO_2 should also measure OH reactivity to unravel possible missing OH reactivity, rather than using the calculated OH reactivity as a lower limit to evaluate the experimental OH and HO_2 data.

Reply

In this campaign, we measured k_{OH} only during 05-19 October by laser the flash photolysis-laser induced fluorescence (LP-LIF) system (Liu et al., 2019), despite the absence of k_{OH} continuous measurement during the period of radical observations (05-28 October 2018). The information on the LP-LIF system is added in Table S1 in the Supplementary Information. The timeseries of the observed and modeled k_{OH} are presented in Fig. S2, in which data gaps were caused by the maintenance of the LP-LIF system. Timeseries of the observed and modeled k_{OH} indicated that the simulations matched well with the observations within the uncertainties during 05-19 October 2018. Therefore, the model can be believed to reproduce the observed k_{OH} values within the whole campaign.

We have added Figure S2 into the Supplementary Information, and revised the description of k_{OH} in Sections 2.1, 3.3, and 4.1, and Table S1 in the Supplementary Information.

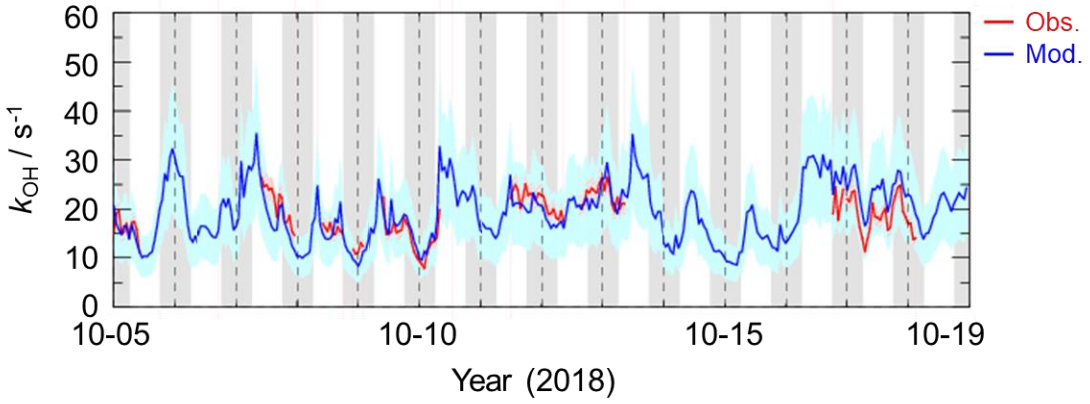

Figure S2: Timeseries of the observed and modeled k_{OH} during 05-19 October 2018. The red and blue areas denote 1-σ uncertainties of the observations and simulations by the model, respectively. The grey areas denote nighttime.

Revision

(1) Section 2.1:

k_{OH} was measured by the laser flash photolysis-laser induced fluorescence (LP-LIF) system.

(2) Section 3.3:

In this campaign, k_{OH} was measured only for several days by the LIP-LIF system, which has been reported in the previous study (Liu et al., 2019). The timeseries of the observed and modeled k_{OH} during 05-19 October 2018 are presented in Fig. S2 in the Supplementary Information. A good agreement between the observed and modeled k_{OH} within the uncertainties was achieved, and thus the model can be believed to reproduce the observed k_{OH} values within the whole campaign.

Moreover, to reflect the k_{OH} in the whole campaign, the modeled values were shown in the k_{OH} diurnal profiles (Fig. 3c) during 05-28 October 2018.

(3) Section 4.1:

As discussed in Section 3.3, it is believed that the model can reproduce the observed k_{OH}. Herein, to conduct the OH experiment budget in the whole campaign, we used the modeled k_{OH} to calculate the OH destruction rate because the k_{OH} was only measured in several days.

2. The reference cell for stabilizing the laser wavelength did not work during the campaign: rather high NO concentrations have therefore been used in the FAGE for HO_2 conversion, and it can be doubted that no interference from RO_2 measurements occurred under these conditions. This is even more strange, as the authors indicate line 99, that there is no obvious difference in HO_2 signal, when changing from 10 to 20 ppm. Does this mean the instrument works already under 100% HO_2 conversion? Then, an RO_2 interference seems very likely. However, 100% conversion efficiency is unlikely, as in a recent paper of the same group, describing a campaign carried out just a few months before in May / June 2018 (Ma et al., OH and HO_2 radicals chemistry at a suburban site during the EXPLORE-YRD

campaign in 2018, ACPD, doi.org/10.5194/acp-2021-1021), a conversion efficiency of 20% was obtained using 5 ppm. Or maybe the authors wanted to say that no obvious difference in HO_2 concentration was observed. Then, the HO_2 conversion rates under different NO concentrations need to be specified.

Reply

Thanks for your helpful suggestions. We have rechecked all the data and made corrections in the revised manuscript.

Revision

(1) Section 2.2:

In this campaign, NO mixing ratios were switched between 25 ppm (low NO mode) and 50 ppm (high NO mode). We calculated the HO_2 conversion rates under the two different NO concentrations by calibrating the PKU-LIF system. HO_2 conversion rates in low NO mode ranged within 80%-95%, while those in high NO mode were over 100%, demonstrating that the HO_2 measurement was affected by RO_2 radicals. Prior studies have reported the relative detection sensitivities (α_{RO_2}) for the major RO_2 species, mainly from alkenes, isoprene and aromatics, when the HO_2 conversion rate was over 100% (Fuchs et al., 2011; Lu et al., 2012; Lu et al., 2013). Therefore, only the HO_2 observations in high NO mode were chosen and they were denoted as $[HO_2^*]$, which was the sum of the true HO_2 concentration and a systematic bias from the mixture of RO_2 species *i* which were detected with different relative sensitivities $\alpha^i_{RO_2}$, as shown in Eq. (1) (Lu et al., 2012). The true HO_2 concentration was difficult to calculated due to the RO_2 concentration measurements and their speciation were not available. Herein, we simulated the HO_2 and HO_2^* concentrations by the model. The interference from RO_2 was estimated to be the difference between the HO_2 and HO_2^* concentrations.

$$[HO_2^*] = [HO_2] + \sum(\alpha^i_{RO_2} \times [RO_2]_i) \quad (1)$$

(2) The figures and descriptions of HO_2 concentration were revised in Section 3.2:

The diurnal maximum of the observed HO_2^*, the modeled HO_2^* and the modeled HO_2 concentrations were 4.2×10^8 cm^{-3}, 6.1×10^8 cm^{-3}, and 4.4×10^8 cm^{-3}, respectively. The difference between the modeled HO_2^* and HO_2 concentrations can be considered a modeled HO_2 interference from RO_2 (Lu et al., 2012). The RO_2 interference was small in the morning, while it became larger in the afternoon. It ranged within 23%-28% during the daytime (08:00-17:00), which was comparable with those in the Backgarden and Yufa sites in China, Borneo rainforest in Malaysia (OP3 campaign, aircraft), and UK (RONOCO campaign, aircraft) (Lu et al., 2012; Lu et al., 2013; Jones et al., 2011; Stone et al., 2014). The observed HO_2^* was overestimated by the model, indicating the HO_2 heterogeneous uptake might have a significant impact during this campaign. The diurnal maximum of HO_2^* concentration observed in Shenzhen was much lower than those observed in the Yufa and Backgarden sites (Lu et al., 2012; Lu et al., 2013; Hofzumahaus et al., 2009).

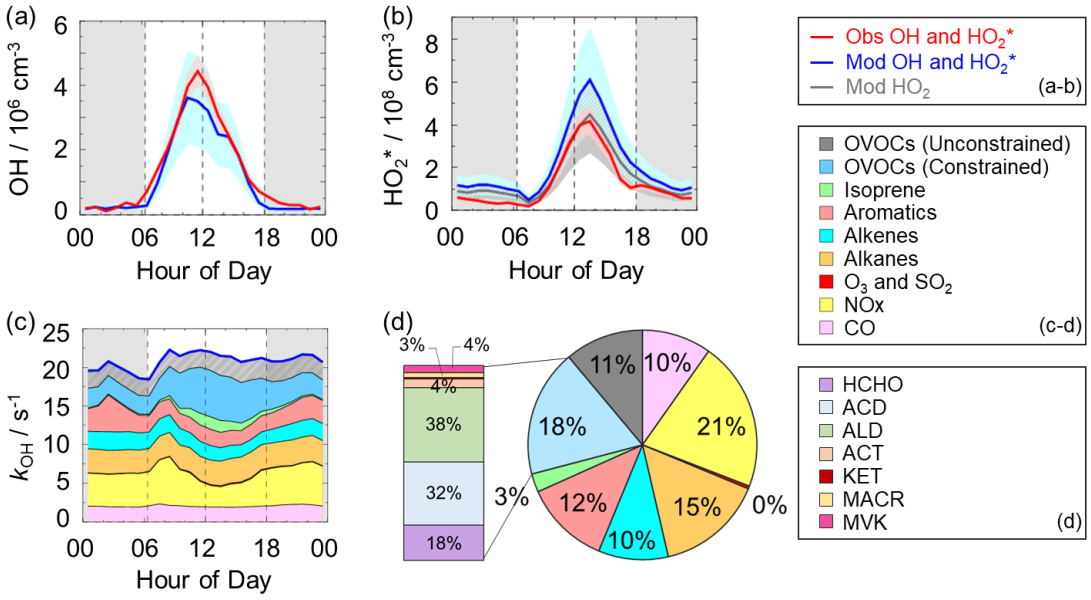

Figure 3: (a-b) The diurnal profiles of the observed and modeled OH, HO_2^* and HO_2 concentrations. (c) The diurnal profiles of the modeled k_{OH}. (d) The composition of the modeled k_{OH}. The red areas in (a-b) denote 1-σ uncertainties of the observed OH and HO_2^* concentrations. The blue areas in (a-b) denote 1-σ uncertainties of the modeled OH and HO_2^* concentrations, and the grey area in (b) denotes 1-σ uncertainties of the modeled HO_2 concentrations. The grey areas in (a-c) denote nighttime. ACD denotes acetaldehydes. ALD denotes the C3 and higher aldehydes. ACT and KET denote acetone and ketones. MACR and MVK denote methacrolein and methyl vinyl ketone.

(3) The timeseries of HO_2 concentrations were revised in Figure S1:

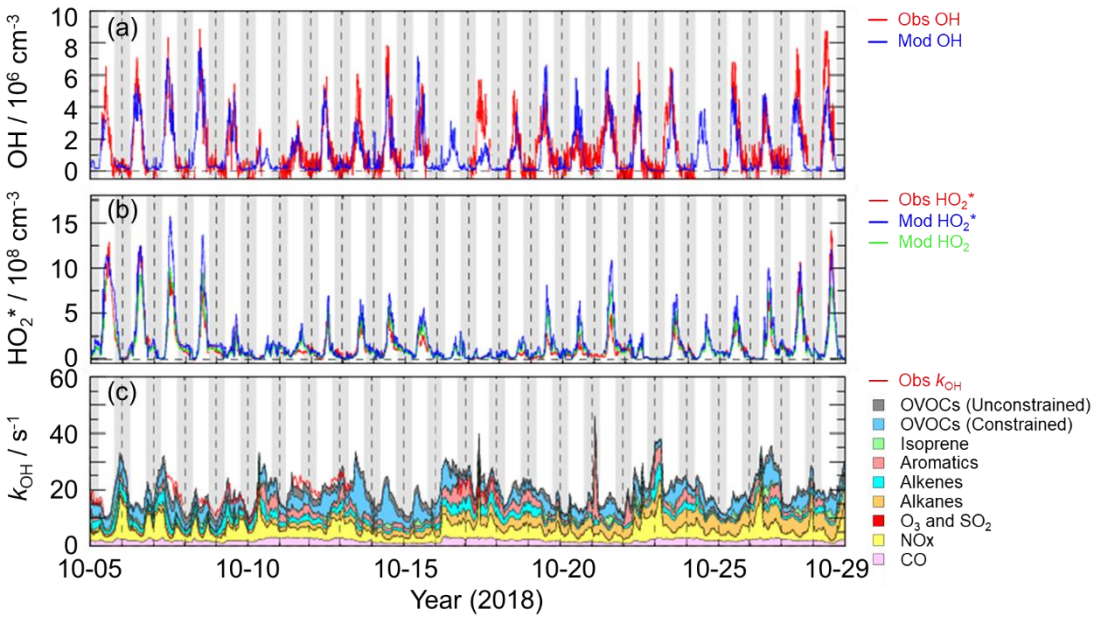

Figure S1: Timeseries of the OH, HO_2^*, HO_2 concentrations and k_{OH} in this study. The grey areas denote nighttime.

(4) The observed HO_2 concentrations can influence the OH experimental budget, so the description in Section 4.1 was revised:

It is noted that the OH production rate was overestimated because we used HO_2^* concentrations instead of HO_2 concentrations here. Thus, the missing OH source was the lower limit here, demonstrating more unknown OH sources need to be further explored.

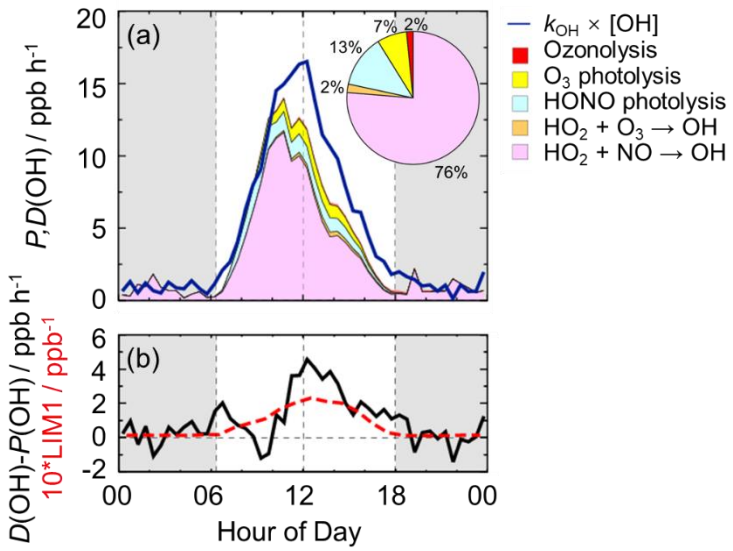

Figure 4: (a) The diurnal profiles of OH production and destruction rates and the proportions of different known sources in the calculated production rate during the daytime. The blue line denotes the OH destruction rate, and the colored areas denote the calculated OH production rates from the known sources. (b) The missing OH source which was the discrepancy between the OH destruction and production rates, and the OH production rate which was ten times the production rate derived from LIM1 mechanism. The grey areas denote nighttime.

(5) The NO dependence of HOx radicals in Fig. 5 was revised:

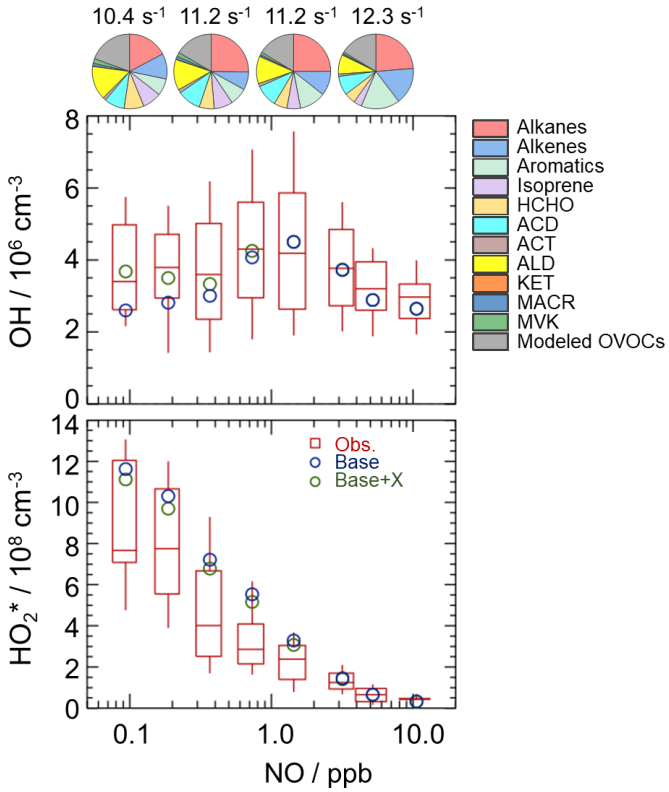

Figure 5: NO dependence of OH and HO_2^* radicals. The red box-whisker plots give the 10%, 25%, median, 75%, and 90% of the HOx observations. The blue circles show the median values of the HOx simulations by the base model, and the green circles show the HOx simulations by the model with X mechanism. Total VOCs reactivity and their organic speciation are presented by pie charts at the different NO intervals at the top. Only daytime values and NO concentration above the detection limit of the instrument were chosen. ACD and ACT denote acetaldehyde and acetone, respectively. ALD denotes the C3 and higher aldehydes. KET denotes ketones. MACR and MVK, which are both the isoprene oxidation products, denote methacrolein and methyl vinyl ketone, respectively.

3. Your model underestimates OH concentration under low NO conditions. I am very surprised that you claim that this is due to an unknown chemical X species, without even loosing a word about possible interferences in the OH measurements. Such increasing OH interferences with decreasing NO concentrations have been identified unequivocally with different FAGE instruments, and an experimental technique has been developed to quantify such possible interferences, this needs to be discussed. And even though some FAGE systems might be more prone to this interference than others, the FAGE community seems to agree on, that occasional measurements with such a pre-injector system are indispensable during field campaigns, especially when low NO concentrations are expected during the campaign. Looking at your above-mentioned paper describing a field campaign a few months before this one, it seems that you had already developed such a pre-injector system at the time of the campaign, because you had already used it. So why did you not use it in this campaign? In my opinion it is idle to discuss OH measurements that are underestimated by the model at low NO conditions, as long as OH-interference to an unknown species has been excluded by experiments using a pre-injector.

Reply

Thanks for your suggestions, the pre-injector system did not be applied in this campaign, but it is believed that the interference in OH measurement in this campaign was negligible by analyzing the PKU-LIF system and the environmental conditions during the campaign.

PKU-LIF system has been applied to measure HOx concentrations for several campaigns. We used the pre-injector system to quantify the possible interferences since 2014, including the campaigns conducted in Wangdu site (Tan et al., 2017), Heshan site (Tan et al., 2019), Huairou site (Tan et al., 2018), Taizhou site (Ma et al., 2022, in review, ACPD), and Chengdu site (Yang et al., 2021). No significant internal interference was found in the prior studies, demonstrating that the accuracy of the PKU-LIF system has been determined for several times.

Moreover, the potential interference may exist when the sampled air contained alkenes, ozone, and BVOCs (Mao et al., 2012; Fuchs et al., 2016; Novelli et al., 2014), indicating the environmental conditions, especially O_3, alkenes and isoprene, are important to the OH interferences. To further explore the potential interference in this campaign, we take Wangdu campaign as an example to compare the major environmental conditions between the prior campaigns and Shenzhen campaign here. During the Wangdu campaign, the chemical modulation tests were conducted on 29 June, 30 June, 02 July, and 05 July 2014, respectively (Tan et al., 2017). The daily mean O_3, alkenes (ethene, butadiene and other anthropogenic dienes, internal alkenes and terminal alkenes) and isoprene concentrations during the daytime

on 29 June were 94.1, 3.8, 1.9 ppb, those on 30 June were 92.2, 2.7, and 1.9 ppb, those on 02 July were 52.9, 1.5, and 0.5 ppb, and those on 05 July were 68.5, 2.4, and 0.9 ppb. The O_3, alkenes and isoprene concentrations on 29 June were highest among those on 29 June, 30 June, 02 July and 05 July, and thus the potential interference on 29 June can be considered the highest among the four days. The results indicated that the potential interference during the daytime in Wangdu was negligible.

Here, we also showed the major parameters related to OH interference in Shenzhen in Table S2 in the Supplementary Information. The daily mean O_3 and isoprene concentrations during the daytime in Shenzhen were within 8.6-91.7 ppb and 0.1-1.0 ppb, which were both lower than those on 29 June in Wangdu. In terms of the alkenes, only 10,16-17 October 2018 in Shenzhen campaign were higher than that observed on 29 June in Wangdu, but the O_3 concentrations on the three days in Shenzhen were only 21.9, 13.9, and 8.6 ppb, and the isoprene concentrations on the three days in Shenzhen were only 0.3, 0.2, and 0.1 ppb, respectively. Overall, the environmental condition in Shenzhen was less conducive to generating potential OH interference than that in Wangdu. Therefore, it is not expected that OH measurement in this campaign was affected by the internal interference.

We have added the description of interval interference in Section 2.2 and the Supplementary Information.

Table S2: The daily mean O_3, alkenes (ethene, butadiene and other anthropogenic dienes, internal alkenes and terminal alkenes) and isoprene concentrations during the daytime (08:00-17:00) in the STORM campaign in this study.

Date / Species	10-05	10-06	10-07	10-08	10-09	10-10	10-11	10-12	10-13	10-14	10-15	10-16
O_3 (ppb)	81.4	83.8	91.7	86.7	48.1	21.9	30.2	42.6	46.8	38.7	40.2	13.9
Alkenes (ppb)	1.4	1.8	3.6	2.3	3.2	5.4	2.9	2.4	2.6	1.4	1.6	4.9
Isoprene (ppb)	0.4	0.4	0.4	0.5	0.4	0.3	0.1	0.3	0.4	0.4	0.6	0.2

Date / Species	10-17	10-18	10-19	10-20	10-21	10-22	10-23	10-24	10-25	10-26	10-27	10-28
O_3 (ppb)	8.6	16.2	39.4	45.8	47.2	25.2	40.9	36.5	55.2	56.5	60.9	60.8
Alkenes (ppb)	4.7	3.2	2.1	1.3	1.2	2.5	2.9	2.7	1.2	3.4	1.7	1.7
Isoprene (ppb)	0.1	0.1	0.5	0.3	0.8	0.8	0.4	0.3	0.5	1.0	0.6	0.8

Revision

(1) Section 2.2:

Additionally, prior studies reported that OH measurement might be affected by the potential interference, when the sampled air contained ozone, alkenes and BVOCs (Mao et al., 2012; Fuchs et al., 2016; Novelli et al., 2014), indicating the environmental conditions are important to the production of interference. The pre-injector is usually used to test the potential OH

interference, and has been applied to our PKU-LIF system to quantify the possible interferences for several campaigns, including the campaigns conducted in Wangdu, Heshan, Huairou, Taizhou and Chengdu sites (Tan et al., 2017; Tan et al., 2019; Tan et al., 2018; Yang et al., 2021). No significant internal interference was found in the prior studies, demonstrating the accuracy of the PKU-LIF system has been determined for several times. Moreover, to further explore the potential interference in this campaign, we compared the major environmental conditions, especially O_3, alkenes and isoprene, between Shenzhen and Wangdu sites, as shown in the Supplementary Information. The environmental condition in Shenzhen was less conducive to generating interference than that in Wangdu, and the details were presented in the Supplementary Information. Therefore, it is not expected that the OH measurements in this campaign were affected by the internal interference.

(2) The detailed information on potential OH interference was added in the Supplementary Information:

We compared the environmental conditions in Shenzhen and Wangdu sites. The chemical modulation tests, which was applied to test the potential OH interference, were conducted on 29 June, 30 June, 02 July and 05 July 2014 in Wangdu (Tan et al., 2017). During the campaign in Wangdu, the daily mean O_3, alkenes (ethene, butadiene and other anthropogenic dienes, internal alkenes and terminal alkenes) and isoprene concentrations during the daytime on 29 June were 94.1, 3.8, 1.9 ppb, those on 30 June were 92.2, 2.7, and 1.9 ppb, those on 02 July were 52.9, 1.5, and 0.5 ppb, and those on 05 July were 68.5, 2.4, and 0.9 ppb, respectively. The O_3, alkenes and isoprene concentrations on 29 June were the highest among those on 29 June, 30 June, 02 July and 05 July, and thus the potential interference on 29 June can be considered the highest among the four days. The chemical modulation results indicated that the potential interference during the daytime in Wangdu was negligible (Tan et al., 2017).

As shown in Table S2, the O_3, alkenes and isoprene concentrations in Shenzhen were within 8.6-91.7 ppb, 1.2-5.4 ppb, and 0.1-1.0 ppb, respectively. The O_3 concentrations in Shenzhen (8.6-91.7 ppb) were lower than those on 29 June (94.1 ppb) and 30 June (92.2 ppb) in Wangdu. Similarly, the isoprene concentrations in Shenzhen (0.1-1.0 ppb) were also lower than those on 29 June (1.9 ppb) and 30 June (1.9 ppb) in Wangdu. In terms of the alkenes, only the concentrations on 10, 16-17 October 2018 (4.7-5.4 ppb) in Shenzhen were higher than that observed on 29 June (3.8 ppb) in Wangdu, but the O_3 concentrations on the three days in Shenzhen were only 21.9, 13.9, and 8.6 ppb, and the isoprene concentrations on the three days in Shenzhen were only 0.3, 0.2, and 0.1 ppb, respectively.

Overall, the environmental condition in Shenzhen was less conducive to generating potential OH interference than that in Wangdu. Therefore, it is not expected that OH measurement in this campaign was affected by the internal interference.

References

Chen, X., Wang, H., Liu, Y., Su, R., Wang, H., Lou, S., and Lu, K.: Spatial characteristics of the nighttime oxidation capacity in the Yangtze River Delta, China, Atmospheric Environment, 208, 150-157, 10.1016/j.atmosenv.2019.04.012, 2019.

Fan, S., Wang, A., Fan, Q., Liu, J., and Wang, B.: ATMOSPHERIC BOUNDARY LAYER CONCEPT MODEL OF THE PEARL RIVER DELTA AND ITS APPLICATION, Journal of Tropical Meteorology,

21, 286-292, 2005.
Fuchs, H., Holland, F., and Hofzumahaus, A.: Measurement of tropospheric RO2 and HO2 radicals by a laser-induced fluorescence instrument, Review of Scientific Instruments, 79, 10.1063/1.2968712, 2008.
Fuchs, H., Bohn, B., Hofzumahaus, A., Holland, F., Lu, K. D., Nehr, S., Rohrer, F., and Wahner, A.: Detection of HO2 by laser-induced fluorescence: calibration and interferences from RO2 radicals, Atmospheric Measurement Techniques, 4, 1209-1225, 10.5194/amt-4-1209-2011, 2011.
Fuchs, H., Tan, Z., Hofzumahaus, A., Broch, S., Dorn, H.-P., Holland, F., Kuenstler, C., Gomm, S., Rohrer, F., Schrade, S., Tillmann, R., and Wahner, A.: Investigation of potential interferences in the detection of atmospheric ROx radicals by laser-induced fluorescence under dark conditions, Atmospheric Measurement Techniques, 9, 1431-1447, 10.5194/amt-9-1431-2016, 2016.
Fuchs, H., Acir, I. H., Bohn, B., Brauers, T., Dorn, H. P., Häseler, R., Hofzumahaus, A., Holland, F., Kaminski, M., Li, X., Lu, K., Lutz, A., Nehr, S., Rohrer, F., Tillmann, R., Wegener, R., and Wahner, A.: OH regeneration from methacrolein oxidation investigated in the atmosphere simulation chamber SAPHIR, Atmos. Chem. Phys., 14, 7895-7908, 10.5194/acp-14-7895-2014, 2014.
Fuchs, H., Albrecht, S., Acir, I.-H., Bohn, B., Breitenlechner, M., Dorn, H.-P., Gkatzelis, G. I., Hofzumahaus, A., Holland, F., Kaminski, M., Keutsch, F. N., Novelli, A., Reimer, D., Rohrer, F., Tillmann, R., Vereecken, L., Wegener, R., Zaytsev, A., Kiendler-Scharr, A., and Wahner, A.: Investigation of the oxidation of methyl vinyl ketone (MVK) by OH radicals in the atmospheric simulation chamber SAPHIR, Atmospheric Chemistry and Physics, 18, 8001-8016, 10.5194/acp-18-8001-2018, 2018.
Fuchs, H., Tan, Z., Lu, K., Bohn, B., Broch, S., Brown, S. S., Dong, H., Gomm, S., Haeseler, R., He, L., Hofzumahaus, A., Holland, F., Li, X., Liu, Y., Lu, S., Min, K.-E., Rohrer, F., Shao, M., Wang, B., Wang, M., Wu, Y., Zeng, L., Zhang, Y., Wahner, A., and Zhang, Y.: OH reactivity at a rural site (Wangdu) in the North China Plain: contributions from OH reactants and experimental OH budget, Atmospheric Chemistry and Physics, 17, 645-661, 10.5194/acp-17-645-2017, 2017.
Gao, M., Li, H., Li, Y., Wei, J., Sun, Y., He, L., and Huang, X.: Source characteristics of water-soluble organic matters in PM_(2.5) in the winter of Shenzhen, China Environmental Science, 38, 4017-4022, 2018.
Heard, D. E. and Pilling, M. J.: Measurement of OH and HO2 in the troposphere, Chemical Reviews, 103, 5163-5198, 10.1021/cr020522s, 2003.
Hofzumahaus, A., Aschmutat, U., Hessling, M., Holland, F., and Ehhalt, D. H.: The measurement of tropospheric OH radicals by laser-induced fluorescence spectroscopy during the POPCORN field campaign, Geophysical Research Letters, 23, 2541-2544, 10.1029/96gl02205, 1996.
Hofzumahaus, A., Rohrer, F., Lu, K., Bohn, B., Brauers, T., Chang, C.-C., Fuchs, H., Holland, F., Kita, K., Kondo, Y., Li, X., Lou, S., Shao, M., Zeng, L., Wahner, A., and Zhang, Y.: Amplified Trace Gas Removal in the Troposphere, Science, 324, 1702-1704, 10.1126/science.1164566, 2009.
Holland, F., Hessling, M., and Hofzumahaus, A.: IN-SITU MEASUREMENT OF TROPOSPHERIC OH RADICALS BY LASER-INDUCED FLUORESCENCE - A DESCRIPTION OF THE KFA INSTRUMENT, Journal of the Atmospheric Sciences, 52, 3393-3401, 10.1175/1520-0469(1995)052<3393:Ismoto>2.0.Co;2, 1995.
Huang, X.-F., Sun, T.-L., Zeng, L.-W., Yu, G.-H., and Luan, S.-J.: Black carbon aerosol characterization in a coastal city in South China using a single particle soot photometer, Atmospheric Environment, 51, 21-28, https://doi.org/10.1016/j.atmosenv.2012.01.056, 2012a.
Huang, X.-F., Chen, D.-L., Lan, Z.-J., Feng, N., He, L.-Y., Yu, G.-H., and Luan, S.-J.: Characterization of organic aerosol in fine particles in a mega-city of South China: Molecular composition, seasonal

variation, and size distribution, Atmospheric Research, 114-115, 28-37, https://doi.org/10.1016/j.atmosres.2012.05.019, 2012b.

Jones, C. E., Hopkins, J. R., and Lewis, A. C.: In situ measurements of isoprene and monoterpenes within a south-east Asian tropical rainforest, Atmospheric Chemistry and Physics, 11, 6971-6984, 10.5194/acp-11-6971-2011, 2011.

Liu, S., Li, X., Shen, X., Zeng, L., Huang, X., Zhu, B., Lin, L., and Lou, S.: Measurement and partition analysis of atmospheric OH reactivity in autumn in Shenzhen, Acta Scientiae Circumstantiae, 39, 3600-3610, 2019.

Lou, S., Holland, F., Rohrer, F., Lu, K., Bohn, B., Brauers, T., Chang, C. C., Fuchs, H., Haeseler, R., Kita, K., Kondo, Y., Li, X., Shao, M., Zeng, L., Wahner, A., Zhang, Y., Wang, W., and Hofzumahaus, A.: Atmospheric OH reactivities in the Pearl River Delta - China in summer 2006: measurement and model results, Atmospheric Chemistry and Physics, 10, 11243-11260, 10.5194/acp-10-11243-2010, 2010.

Lu, K. D., Hofzumahaus, A., Holland, F., Bohn, B., Brauers, T., Fuchs, H., Hu, M., Haeseler, R., Kita, K., Kondo, Y., Li, X., Lou, S. R., Oebel, A., Shao, M., Zeng, L. M., Wahner, A., Zhu, T., Zhang, Y. H., and Rohrer, F.: Missing OH source in a suburban environment near Beijing: observed and modelled OH and HO2 concentrations in summer 2006, Atmospheric Chemistry and Physics, 13, 1057-1080, 10.5194/acp-13-1057-2013, 2013.

Lu, K. D., Rohrer, F., Holland, F., Fuchs, H., Bohn, B., Brauers, T., Chang, C. C., Haeseler, R., Hu, M., Kita, K., Kondo, Y., Li, X., Lou, S. R., Nehr, S., Shao, M., Zeng, L. M., Wahner, A., Zhang, Y. H., and Hofzumahaus, A.: Observation and modelling of OH and HO2 concentrations in the Pearl River Delta 2006: a missing OH source in a VOC rich atmosphere, Atmospheric Chemistry and Physics, 12, 1541-1569, 10.5194/acp-12-1541-2012, 2012.

Mao, J., Ren, X., Zhang, L., Van Duin, D. M., Cohen, R. C., Park, J. H., Goldstein, A. H., Paulot, F., Beaver, M. R., Crounse, J. D., Wennberg, P. O., DiGangi, J. P., Henry, S. B., Keutsch, F. N., Park, C., Schade, G. W., Wolfe, G. M., Thornton, J. A., and Brune, W. H.: Insights into hydroxyl measurements and atmospheric oxidation in a California forest, Atmospheric Chemistry and Physics, 12, 8009-8020, 10.5194/acp-12-8009-2012, 2012.

Novelli, A., Hens, K., Ernest, C. T., Kubistin, D., Regelin, E., Elste, T., Plass-Duelmer, C., Martinez, M., Lelieveld, J., and Harder, H.: Characterisation of an inlet pre-injector laser-induced fluorescence instrument for the measurement of atmospheric hydroxyl radicals, Atmospheric Measurement Techniques, 7, 3413-3430, 10.5194/amt-7-3413-2014, 2014.

Peeters, J., Nguyen, T. L., and Vereecken, L.: HOx radical regeneration in the oxidation of isoprene, Physical Chemistry Chemical Physics, 11, 5935-5939, 10.1039/b908511d, 2009.

Peeters, J., Muller, J.-F., Stavrakou, T., and Vinh Son, N.: Hydroxyl Radical Recycling in Isoprene Oxidation Driven by Hydrogen Bonding and Hydrogen Tunneling: The Upgraded LIM1 Mechanism, Journal of Physical Chemistry A, 118, 8625-8643, 10.1021/jp5033146, 2014.

Song, H., Lu, K., Dong, H., Tan, Z., Chen, S., Zeng, L., and Zhang, Y.: Reduced Aerosol Uptake of Hydroperoxyl Radical May Increase the Sensitivity of Ozone Production to Volatile Organic Compounds, Environmental Science & Technology Letters, 9, 22-29, 10.1021/acs.estlett.1c00893, 2022.

Stevens, P. S., Mather, J. H., Brune, W. H., Eisele, F., Tanner, D., Jefferson, A., Cantrell, C., Shetter, R., Sewall, S., Fried, A., Henry, B., Williams, E., Baumann, K., Goldan, P., and Kuster, W.: HO2/OH and RO(2)/HO2 ratios during the Tropospheric OH Photochemistry Experiment: Measurement and theory, Journal of Geophysical Research-Atmospheres, 102, 6379-6391, 10.1029/96jd01704, 1997.

Stone, D., Evans, M. J., Walker, H., Ingham, T., Vaughan, S., Ouyang, B., Kennedy, O. J., McLeod, M.

W., Jones, R. L., Hopkins, J., Punjabi, S., Lidster, R., Hamilton, J. F., Lee, J. D., Lewis, A. C., Carpenter, L. J., Forster, G., Oram, D. E., Reeves, C. E., Bauguitte, S., Morgan, W., Coe, H., Aruffo, E., Dari-Salisburgo, C., Giammaria, F., Di Carlo, P., and Heard, D. E.: Radical chemistry at night: comparisons between observed and modelled HOx, NO3 and N2O5 during the RONOCO project, Atmospheric Chemistry and Physics, 14, 1299-1321, 10.5194/acp-14-1299-2014, 2014.

Taketani, F., Kanaya, Y., Pochanart, P., Liu, Y., Li, J., Okuzawa, K., Kawamura, K., Wang, Z., and Akimoto, H.: Measurement of overall uptake coefficients for HO2 radicals by aerosol particles sampled from ambient air at Mts. Tai and Mang (China), Atmospheric Chemistry and Physics, 12, 11907-11916, 10.5194/acp-12-11907-2012, 2012.

Tan, Z., Lu, K., Hofzumahaus, A., Fuchs, H., Bohn, B., Holland, F., Liu, Y., Rohrer, F., Shao, M., Sun, K., Wu, Y., Zeng, L., Zhang, Y., Zou, Q., Kiendler-Scharr, A., Wahner, A., and Zhang, Y.: Experimental budgets of OH, HO2, and RO2 radicals and implications for ozone formation in the Pearl River Delta in China 2014, Atmospheric Chemistry and Physics, 19, 7129-7150, 10.5194/acp-19-7129-2019, 2019.

Tan, Z., Hofzumahaus, A., Lu, K., Brown, S. S., Holland, F., Huey, L. G., Kiendler-Scharr, A., Li, X., Liu, X., Ma, N., Min, K.-E., Rohrer, F., Shao, M., Wahner, A., Wang, Y., Wiedensohler, A., Wu, Y., Wu, Z., Zeng, L., Zhang, Y., and Fuchs, H.: No Evidence for a Significant Impact of Heterogeneous Chemistry on Radical Concentrations in the North China Plain in Summer 2014, Environmental Science & Technology, 54, 5973-5979, 10.1021/acs.est.0c00525, 2020.

Tan, Z., Fuchs, H., Lu, K., Hofzumahaus, A., Bohn, B., Broch, S., Dong, H., Gomm, S., Haeseler, R., He, L., Holland, F., Li, X., Liu, Y., Lu, S., Rohrer, F., Shao, M., Wang, B., Wang, M., Wu, Y., Zeng, L., Zhang, Y., Wahner, A., and Zhang, Y.: Radical chemistry at a rural site (Wangdu) in the North China Plain: observation and model calculations of OH, HO2 and RO2 radicals, Atmospheric Chemistry and Physics, 17, 663-690, 10.5194/acp-17-663-2017, 2017.

Tan, Z., Rohrer, F., Lu, K., Ma, X., Bohn, B., Broch, S., Dong, H., Fuchs, H., Gkatzelis, G. I., Hofzumahaus, A., Holland, F., Li, X., Liu, Y., Liu, Y., Novelli, A., Shao, M., Wang, H., Wu, Y., Zeng, L., Hu, M., Kiendler-Scharr, A., Wahner, A., and Zhang, Y.: Wintertime photochemistry in Beijing: observations of ROx radical concentrations in the North China Plain during the BEST-ONE campaign, Atmospheric Chemistry and Physics, 18, 12391-12411, 10.5194/acp-18-12391-2018, 2018.

Wang, X., Wang, H., Xue, L., Wang, T., Wang, L., Gu, R., Wang, W., Tham, Y. J., Wang, Z., Yang, L., Chen, J., and Wang, W.: Observations of N2O5 and ClNO2 at a polluted urban surface site in North China: High N2O5 uptake coefficients and low ClNO2 product yields, Atmospheric Environment, 156, 125-134, 10.1016/j.atmosenv.2017.02.035, 2017.

Whalley, L. K., Slater, E. J., Woodward-Massey, R., Ye, C., Lee, J. D., Squires, F., Hopkins, J. R., Dunmore, R. E., Shaw, M., Hamilton, J. F., Lewis, A. C., Mehra, A., Worrall, S. D., Bacak, A., Bannan, T. J., Coe, H., Percival, C. J., Ouyang, B., Jones, R. L., Crilley, L. R., Kramer, L. J., Bloss, W. J., Vu, T., Kotthaus, S., Grimmond, S., Sun, Y., Xu, W., Yue, S., Ren, L., Acton, W. J. F., Hewitt, C. N., Wang, X., Fu, P., and Heard, D. E.: Evaluating the sensitivity of radical chemistry and ozone formation to ambient VOCs and NOx in Beijing, Atmospheric Chemistry and Physics, 21, 2125-2147, 10.5194/acp-21-2125-2021, 2021.

Yang, X., Lu, K., Ma, X., Liu, Y., Wang, H., Hu, R., Li, X., Lou, S., Chen, S., Dong, H., Wang, F., Wang, Y., Zhang, G., Li, S., Yang, S., Yang, Y., Kuang, C., Tan, Z., Chen, X., Qiu, P., Zeng, L., Xie, P., and Zhang, Y.: Observations and modeling of OH and HO2 radicals in Chengdu, China in summer 2019, The Science of the total environment, 772, 144829-144829, 10.1016/j.scitotenv.2020.144829, 2021.

Zhang, Y. H., Hu, M., Zhong, L. J., Wiedensohler, A., Liu, S. C., Andreae, M. O., Wang, W., and Fan, S.

J.: Regional Integrated Experiments on Air Quality over Pearl River Delta 2004 (PRIDE-PRD2004): Overview, Atmospheric Environment, 42, 6157-6173, 10.1016/j.atmosenv.2008.03.025, 2008.

Zhou, J., Murano, K., Kohno, N., Sakamoto, Y., and Kajii, Y.: Real-time quantification of the total HO2 reactivity of ambient air and HO2 uptake kinetics onto ambient aerosols in Kyoto (Japan), Atmospheric Environment, 223, 10.1016/j.atmosenv.2020.117189, 2020.

Zhou, J., Sato, K., Bai, Y., Fukusaki, Y., Kousa, Y., Ramasamy, S., Takami, A., Yoshino, A., Nakayama, T., Sadanaga, Y., Nakashima, Y., Li, J., Murano, K., Kohno, N., Sakamoto, Y., and Kajii, Y.: Kinetics and impacting factors of HO2 uptake onto submicron atmospheric aerosols during the 2019 Air QUAlity Study (AQUAS) in Yokohama, Japan, Atmospheric Chemistry and Physics, 21, 12243-12260, 10.5194/acp-21-12243-2021, 2021.

Response to Reviewer comment #2:

General comments:

This manuscript describes OH and HO_2 measurements in Shenzhen during Autumn 2018 and the skills of a photochemical box model to reproduce the observed radical levels when constrained with simultaneous observations of key reactants, to test the atmospheric photochemistry theory. The results showed that the model underestimated OH levels while it reproduced HO_2 levels well. Missing recycling from HO_2 to OH by species X was suggested, while the required levels of X were not very high (0.1 ppb). The atmospheric oxidation capacity was calculated on the observation basis and compared with the O_3 formation rate. The results, though not including OH reactivity measurements, are worth to be added to those from numbers of previous field studies, for future diagnostics of missing processes in the model. Though the number of field studies in China has been increasing, the chemical conditions are very different among the studies and more field evidence is necessary. However, for this purpose, clarification is necessary at several points. First, uncertainty analysis needs to be provided for both observations and model simulations, particularly when the authors claim introduction of X to explain the model's underestimation of the OH levels. Second, the authors cited values or results from previous studies for comparison but in-depth analysis/discussion across the studies were not provided in search for missing processes. The authors should specify the important characteristics of the conditions studied during this campaign and what is enabled with the observational results. Third, I am afraid that the major OH term of the atmospheric oxidation capacity is not very innovative; it is just the OH reactivity multiplied to the OH concentrations, i.e., OH loss rate, and thus it is very natural that it correlates with $F(O_3)$, i.e., the HO_2/RO_2 + NO rate, when the OH loss produces RO_2/HO_2 and the peroxy radicals undergo reactions with NO. Overall, I would suggest major revisions regarding the points above and the following specific comments.

Reply

We thank you for all the valuable comments and suggestions which are helpful for the important guiding significance to us. We have taken all these comments and suggestions into account as follows:

(1) First, we added the uncertainty analysis for the observed and modeled radical concentrations, as shown in the revised figure in the Reply to Question 11.

(2) Second, the comparisons of radical concentrations and chemical conditions between this campaign and other campaigns were added, as shown in Reply to Question 3 and Question 9. Additionally, we explored the influencing factors of missing OH sources and further evaluated the contribution of isoprene chemistry to radical sources.

(3) Third, as for the analysis of AOC, we added the NO dependence of the ratio of $P(O_3)$ to AOC to explore the ozone formation from VOCs oxidation, as shown in the Reply to Question 17.

Below are our responses to the specific comments, highlighted in blue, with changes to the manuscript highlighted in green.

Specific comments:

1. Page 1, Line 26. Definition of the atmospheric oxidation capacity should be briefly mentioned in Abstract.

Reply

We have added the definition of atmospheric oxidation capacity in the Abstract, and we changed the unit of AOC according to Question 17.

Revision

As the sum of the respective oxidation rates of the pollutants via reactions with oxidants, the atmospheric oxidation capacity was evaluated, with a peak of 11.8 ppb h^{-1} around noontime.

2. Page 1, Line 26. x -> times character.

Reply

As the Reply to Question 1, the '×' here has been deleted. Besides, we have revised the character of '×' in the whole manuscript.

3. Page 2, Line 56. What are the important chemical conditions for this STORM campaign, in terms of differences from previous studies done in PRD, for example, city center/rural, NOx/BVOC levels, seasons etc.? From the inset map of Figure 1, I was not able to see if the site was in the city or in a rural region.

Reply

We have added the description of the site in Section 2.1 and the comparison of environmental conditions between the three campaigns conducted in PRD (Backgarden, Heshan, and Shenzhen) in Section 3.1.

Revision

(1) Section 2.1:

As shown in Fig. 1, the Shenzhen site, which belongs to the urban site, is located in the university town, and is surrounded by residential and commercial areas.

Overall, this site has no significant local pollution sources nearby, but can represent the urban pollution characteristics (Huang et al., 2012b; Huang et al., 2012a; Gao et al., 2018).

(2) Section 3.1:

Moreover, we compared the environmental conditions between the Backgarden (rural site), Heshan (suburban site), and Shenzhen (urban site) campaigns conducted in PRD in Table S3 in the Supplementary Information. No significant discrepancy in temperature was found in the Shenzhen and Heshan campaigns, which were both conducted in autumn. The temperature in the Backgarden campaign conducted in summer was higher than those in Shenzhen and Heshan. The relative humidity in Shenzhen and Backgarden was higher than that in Heshan. Compared to the chemical conditions in the Heshan campaign conducted in autumn as well, the

concentrations of CO, NO, NO_2, HONO, alkenes, aromatics, and HCHO in Shenzhen were lower, which might be because there were no significant local pollution sources nearby in the Shenzhen site although it was an urban site. However, the concentration of O_3 which is the typical secondary pollutant in Shenzhen was higher than that in Heshan. Compared to the environmental conditions in Heshan, the higher O_3 concentration in Shenzhen might benefit from the weather condition which was characterized by the stronger solar radiation and slightly higher temperatures.

Table S3: The meteorological parameters, photolysis rate constant, and concentrations of trace gases in the Backgarden, Heshan, and Shenzhen campaigns.

Parameters	Backgarden (2006, summer)	Heshan (2014, autumn)	Shenzhen (2018, autumn)
Temperature (K)	303.9	295.1	297.5
Pressure (hPa)	1002.9	1010.1	1009.7
Relative humidity (%)	72.3	66	75.4
$j(O^1D)$ / 10^{-5} s^{-1}	3.6	1.3	1.8
$j(NO_2)$ / 10^{-3} s^{-1}	7.6	4.1	5.7
CO / ppb	948.6	642.7	386.6
NO / ppb	5.7	3.6	2.6
NO_2 / ppb	14.3	18.7	14.9
O_3 / ppb	32.3	26.5	32.2
HONO / ppb	1.0	1.4	0.5
Alkanes / ppb	13.9	16.7	20.2
Alkenes / ppb	2.1	6.0	2.8
Aromatics / ppb	11.2	8.6	8.2
HCHO / ppb	--	5.9	3.3

Note that:

The $j(O^1D)$ and $j(NO_2)$ were the mean values during the noontime, and other parameters were the mean values during the whole day.

4. Page 3, line 68. The coordinate should be 22.60 deg N and 113.97 deg E? (decimal points)

Reply

We revised the coordinate as your suggestions.

5. Page 4, lines 89-96. Any literature to which the readers refer for further information of the specific FAGE instrument? Also, the uncertainty in OH and HO_2 measurements should be quantified.

Reply

We added more references on the FAGE instrument and added the HOx measurement uncertainties in the manuscript which have been represented in Table S1 in the Supplementary Information.

Revision

Section 2.2:

Further detailed information on the instrument can be found in previous studies (Heard and Pilling, 2003; Fuchs et al., 2008; Holland et al., 1995; Hofzumahaus et al., 1996; Fuchs et al., 2011).

Overall, the measurement uncertainties of OH and HO_2^* radicals were 11% and 15%, respectively, as shown in Table S1 in the Supplementary Information.

6. Page 4, line 107. Did the author mean latest isoprene chemistry?

Reply

Yes, RACM2-LIM1 means the latest isoprene chemistry. We wrote the wrong word 'lasted', and revised it to 'latest'.

Revision

In this work, we conducted the radical closure experiment based on the Regional Atmospheric Chemical Mechanism updated with the latest isoprene chemistry (RACM2-LIM1).

7. Page 4, line 110. What are the "long-lived" species? Readers may think CO_2 or CH_4 as long-lived, which are not surely supposed in this context. I believe they are the modeled carbonyls/peroxides etc. But did they reach steady state within 2 days of integration? Did the authors assume a fast turnover time constant (dilution constant) for them? If so, any justification of the assumption?

Reply

The expression was not accurate, and thanks for your suggestion. Herein, the spin-up for the model is used to let the unconstrained species, which are mainly some intermediate species, approach the steady state relative to the constrained species. We have revised the description in Section 2.3.

Revision

The model was operated in time-dependent mode with a 5-min time resolution, and a 2-d spin-up time which was to make the unconstrained species approach the steady state relative to the constrained species.

8. Page 4, lines 118. It is confusing to mention the observed k_OH from other studies, as that measurement was not available for this particular study.

Reply

In this campaign, we measured k_{OH} only during 05-19 October by the laser flash photolysis-laser induced fluorescence (LP-LIF) system (Liu et al., 2019), despite the absence of k_{OH} continuous measurement during the period of radical observations (05-28 October 2018). The information on LP-LIF is shown in Table S1 in the Supplementary Information. The timeseries

of the observed and modeled k_{OH} are presented in Fig. S2, in which data gaps were caused by the maintenance of the LP-LIF system. Timeseries of the observed and modeled k_{OH} indicated that the simulations matched well with the observations within the uncertainties during 08-12 October 2018. Therefore, the model can be believed to reproduce the observed k_{OH} values within the whole campaign.

We have added Figure S2 into the Supplementary Information, and revised the description of k_{OH} in Sections 2.1, 3.3, and 4.1, and Table S1 in the Supplementary Information.

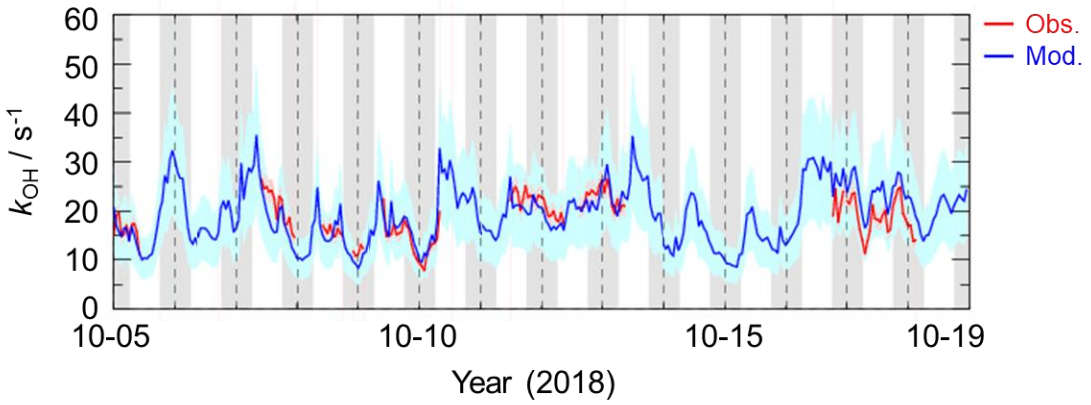

Figure S2: Timeseries of the observed and modeled k_{OH} during 05-19 October 2018. The red and blue areas denote 1-σ uncertainties of the observations and simulations by the model, respectively. The grey areas denote nighttime.

Revision

(6) Section 2.1:

k_{OH} was measured by the laser flash photolysis-laser induced fluorescence (LP-LIF) system.

(7) Section 3.3:

In this campaign, k_{OH} was measured only for several days by the LIP-LIF system, which has been reported in the previous study (Liu et al., 2019). The timeseries of the observed and modeled k_{OH} during 05-19 October 2018 are presented in Fig. S2 in the Supplementary Information. A good agreement between the observed and modeled k_{OH} within the uncertainties was achieved, and thus the model can be believed to reproduce the observed k_{OH} values within the whole campaign.

Moreover, to reflect the k_{OH} in the whole campaign, the modeled values were shown in the k_{OH} diurnal profiles (Fig. 3c) during 05-28 October 2018.

(8) Section 4.1:

As discussed in Section 3.3, it is believed that the model can reproduce the observed k_{OH}. Herein, to conduct the OH experiment budget in the whole campaign, we used the modeled k_{OH} to calculate the OH destruction rate because the k_{OH} was only measured in several days.

9. Page 8, Line 181. More discussion is preferred; what are the similarities and what are the differences to/from the previous studies in PRD?

Reply

The comparison between the three studies in Shenzhen, Heshan and Backgarden sites in PRD did be necessary. Here, we added the comparisons of HOx concentrations, k_{OH} and missing OH sources in Sections 3.2, 3.3 and 4.2.2, respectively.

Revision

(1) Section 3.2:

Compared to the other campaigns conducted in PRD (Backgarden and Heshan), the diurnal maximum of the observed OH concentration in Shenzhen was equal to that observed in Heshan, and much lower than that observed in Backgarden where the observed OH concentration was nearly 15×10^6 cm^{-3} (Hofzumahaus et al., 2009; Tan et al., 2019). The higher OH concentration in Backgarden site was closely correlated to the stronger solar radiation, as shown in Table S3 in the Supplementary Information.

The diurnal maximum of HO_2^* concentration observed in Shenzhen was slightly higher than that observed in Heshan (3×10^8 cm^{-3}), but much small than that observed in Backgarden (18×10^8 cm^{-3}) (Hofzumahaus et al., 2009; Tan et al., 2019; Lu et al., 2012).

(2) Section 3.3:

Compared to the k_{OH} variation in Shenzhen, the k_{OH} observed in Backgarden and Heshan sites in PRD showed a stronger diurnal variation, with a minimum value at around noontime and a maximum value at daybreak. The k_{OH} ranges in Backgarden and Heshan were 20-50 s^{-1} and 22-32 s^{-1} (Lou et al., 2010; Tan et al., 2019). Similar with the good agreement between the observed and modeled k_{OH} during the several days in Shenzhen, the observed k_{OH} in Backgarden was matched well with the modeled k_{OH} which has included the OVOCs reactivity. In terms of the k_{OH} in Heshan, Tan et al. (2019) reported that only half of the observed k_{OH} was explained by the calculated k_{OH} which was calculated from the measured trace gas concentrations. The missing k_{OH} in Heshan was likely caused by unmeasured VOCs, demonstrating the necessary to measure more abundant VOCs species, especially OVOCs species.

(3) Section 4.2.2:

Compared to Shenzhen site, the X concentration in the Backgarden and Heshan sites in PRD were higher, which might be affected by the different air masses in the three sites. The k_{OH} in Shenzhen site was much lower than those in Backgarden and Heshan sites, and the weaker variation of k_{OH} in Shenzhen was observed. Under the influence of the East Asian monsoon, the prevailing wind for PRD area is mostly southerly during the summer months and mostly northerly during the winter months (Fan et al., 2005; Zhang et al., 2008). The Backgarden site is located in Guangzhou, and the Heshan site is located in Jiangmen. The two cities are along the north-south axis, and thus the air masses of the Backgarden and Heshan sites are intimately linked with each other, while the air mass in Shenzhen is more similar to Hongkong (Zhang et al., 2008).

10. Page 8, Figure 3c and d. The fraction of the modeled OVOCs is fairly large. More explanation is needed what these species are and how their concentrations are justified.

Reply:

Large fraction of OVOCs reactivities in k_{OH} was also found in some previous studies (Lou et al., 2010; Lu et al., 2013; Fuchs et al., 2017; Whalley et al., 2021). About 50% of k_{OH} was explained by OVOCs in Backgarden site. HCHO, acetaldehydes and higher aldehydes, and oxygenated isoprene products were the most important OH reactants in OVOCs, with a contribution of 30-40%, and other 10-20% came from other oxygenated compounds (ketones, dicarbonyl compounds, alcohols, hydroperoxides, nitrates etc.) (Lou et al., 2010). HCHO, acetaldehydes, MVK, MVCR and glyoxal accounted for one-third of the total k_{OH} in Wangdu site (Fuchs et al., 2017).

In this study, we measured several OVOCs species, including HCHO, acetaldehydes (ACD) and higher aldehydes (ALD), acetone (ACT), ketones (KET) and isoprene oxidation products (MACR and MVK), so we constrained these species in the model and revised the composition of k_{OH} in Fig. 3(c-d). The constrained OVOCs species accounted for 18% in the total k_{OH}, where HCHO, ACD, and ALD were the major contributors, with contributions of 18%, 32%, and 38% to the constrained OVOCs, respectively. The contribution of aldehydes to the total k_{OH} in this study (16%) was larger than that in Beijing (Whalley et al., 2021) and smaller with that in Wangdu (Fuchs et al., 2017). The unconstrained OVOCs reactivity, mainly from the model-generated intermediate species (glyoxal, methylglyoxal, methyl ethyl ketone, methanol, etc.), accounted for 11% in the total k_{OH} in this campaign.

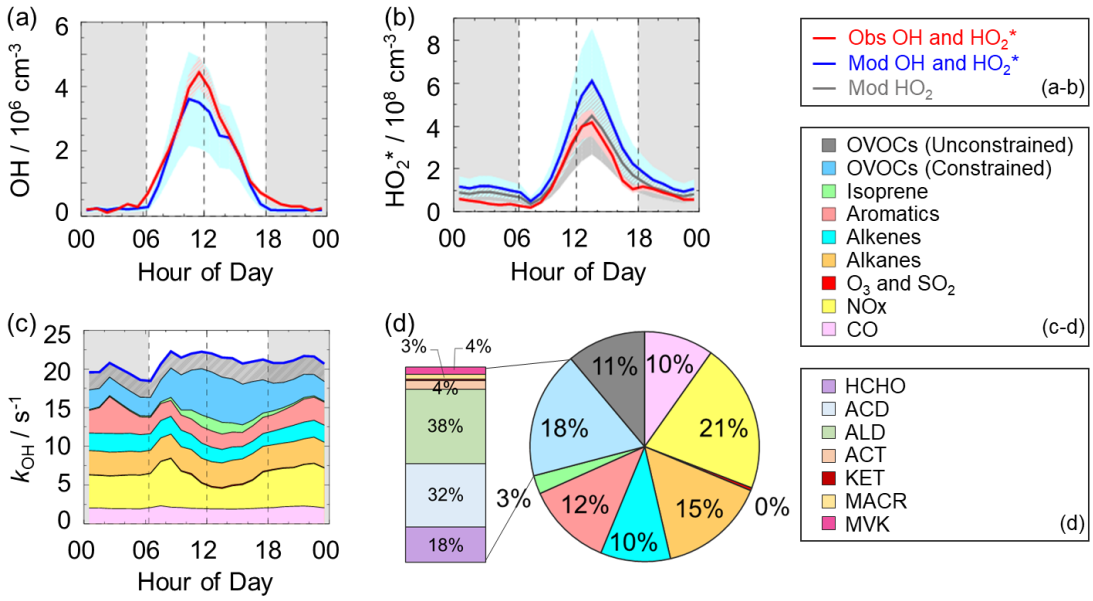

Figure 3: (a-b) The diurnal profiles of the observed and modeled OH, HO_2^* and HO_2 concentrations. (c) The diurnal profiles of the modeled k_{OH}. (d) The composition of the modeled k_{OH}. The red areas in (a-b) denote 1-σ uncertainties of the observed OH and HO_2^* concentrations. The blue areas in (a-b) denote 1-σ uncertainties of the modeled OH and HO_2^* concentrations, and the grey area in (b) denotes 1-σ uncertainties of the modeled HO_2 concentrations. The grey areas in (a-c) denote nighttime. ACD denotes acetaldehydes. ALD denotes the C3 and higher aldehydes. ACT and KET denote acetone and ketones. MACR and MVK denote methacrolein and methyl vinyl ketone.

As for the unmeasured OVOCs species, it is difficult to justifying their concentrations, since the in-situ measuremnts of these species are missing, but the plausibility for them can be

checked. In this study, the mean k_{OH} value was 20.8 s^{-1}, and thus the reactivitiy of the unconstrained OVOCs species was 2.3 s^{-1}. In the Backgarden site, the reactivity of oxygenated compounds (ketones, dicarbonyl compounds, alcohols, hydroperoxides, nitrates etc.), which accounted for 10%-20% of the total k_{OH}, was about 3.3-6.6 s^{-1} (the mean k_{OH} was about 32.9 s^{-1}) (Lou et al., 2010). The reactivity of these OVOCs species in our study were of similar magnitude as the reported by Lou et al. (2010), indicating the modeled unconstrained OVOCs reactivitys can be believed in this study.

Revision:

Section 3.3

Compared with inorganics reactivity, the larger fraction of k_{OH} came from the VOCs group, with a contribution of 69% to k_{OH}. The contribution of alkanes, alkenes, and aromatics were 15%, 10%, and 12%, respectively. The isoprene reactivity related to temperature was mainly concentrated during the daytime, whereas the aromatics reactivity at night was higher. As for the OVOCs species, we measured several OVOCs species, including HCHO, acetaldehydes (ACD) and higher aldehydes (ALD), acetone (ACT), ketones (KET) and isoprene oxidation products (MACR and MVK), so we constrained these species in the model. The constrained OVOCs species accounted for 18% in the total k_{OH}, where HCHO, ACD, and ALD were the major contributors, with contributions of 18%, 32%, and 38% to the constrained OVOCs, respectively. The contribution of aldehydes in this study (16%) was larger than that in Beijing (Whalley et al., 2021) and smaller with that in Wangdu (Fuchs et al., 2017). The remaining reactivity was attributed to the unconstrained OVOCs reactivity, which came from the model-generated intermediate species (glyoxal, methylglyoxal, methyl ethyl ketone, methanol, etc.), with a contribution of 11% to the total k_{OH}. Large fraction of OVOCs reactivities in k_{OH} was also found in some previous studies (Lou et al., 2010; Lu et al., 2013; Fuchs et al., 2017; Whalley et al., 2021). About 50% of k_{OH} was explained by OVOCs in Backgarden site, and HCHO, ACD and ALD, and oxygenated isoprene products were the most important OH reactants in OVOCs, with a contribution of 30-40%, and other 10-20% came from other oxygenated compounds (ketones, dicarbonyl compounds, alcohols, hydroperoxides, nitrates etc.) (Lou et al., 2010). HCHO, ACD, MVK, MVCR and glyoxal accounted for one-third of the total k_{OH} in Wangdu site (Fuchs et al., 2017). The large unconstrained OVOCs reactivity indicated it is necessary to measure more VOCs species in the future.

11. Page 8, line 188. Were the aerosol surface concentrations measured? Can the authors discuss maximum possible uptake coefficient from the surface concentrations?

Reply

The aerosol surface concentrations observations were not measured in this campaign, but they can be estimated roughly by multiplying the mass concentration of $PM_{2.5}$ by 20 (Chen et al., 2019; Wang et al., 2017). Herein, we discussed the possible HO_2 uptake coefficient from the surface concentrations.

First, we note that we rechecked our data and revised the description of HO_2 observations. In this campaign, NO mixing ratios were switched between 25 ppm (low NO mode) and 50 ppm (high NO mode). We calculated the HO_2 conversion rates under the two different NO

concentrations by calibrating the PKU-LIF system. HO_2 conversion rates in low NO mode ranged within 80%-95%, while those in high NO mode were over 100%, demonstrating that the HO_2 measurement was affected by RO_2 radicals. Prior studies have reported the relative detection sensitivities (α_{RO_2}) for the major RO_2 species, mainly from alkenes, isoprene and aromatics, when the HO_2 conversion rate was over 100% (Fuchs et al., 2011; Lu et al., 2012; Lu et al., 2013). Therefore, only the HO_2 observations in high NO mode were chosen and they were denoted as $[HO_2^*]$, which was the sum of the true HO_2 concentration and a systematic bias from the mixture of RO_2 species i which were detected with different relative sensitivities $\alpha^i_{RO_2}$, as shown in Eq. (1) (Lu et al., 2012). The true HO_2 concentration was difficult to calculated due to the RO_2 concentration measurements and their speciation were not available. Herein, we simulated the HO_2 and HO_2^* concentrations by the model. The interference from RO_2 was estimated to be the difference between the HO_2 and HO_2^* concentrations.

$$[HO_2^*] = [HO_2] + \sum(\alpha^i_{RO_2} \times [RO_2]_i) \quad (1)$$

The figures and descriptions of HO_2 concentration were revised in Section 3.2:

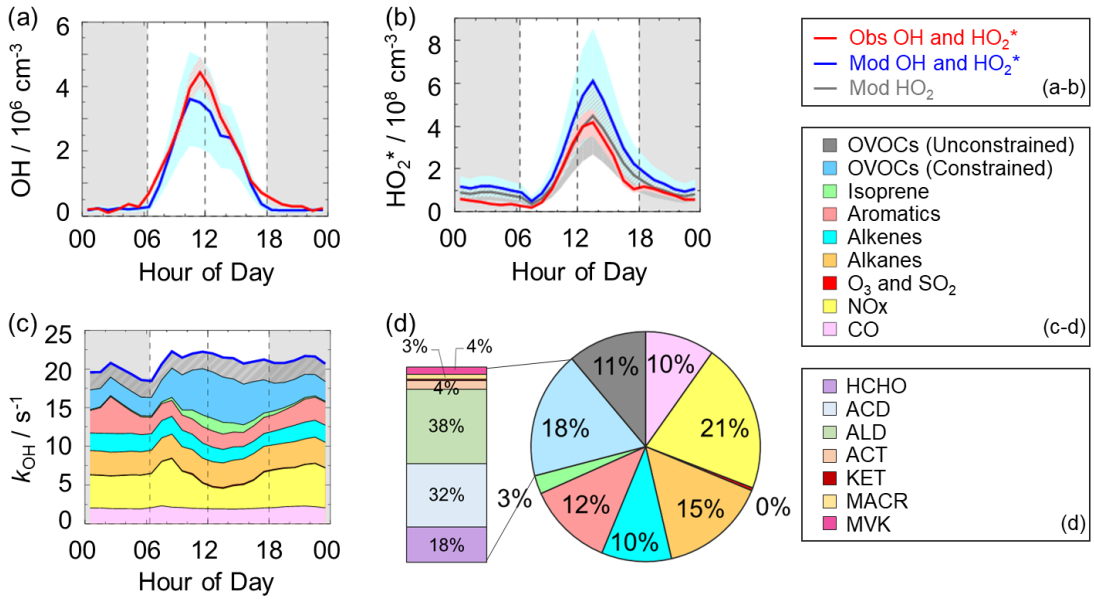

Figure 3: (a-b) The diurnal profiles of the observed and modeled OH, HO_2^* and HO_2 concentrations. (c) The diurnal profiles of the modeled k_{OH}. (d) The composition of the modeled k_{OH}. The red areas in (a-b) denote 1-σ uncertainties of the observed OH and HO_2^* concentrations. The blue areas in (a-b) denote 1-σ uncertainties of the modeled OH and HO_2^* concentrations, and the grey area in (b) denotes 1-σ uncertainties of the modeled HO_2 concentrations. The grey areas in (a-c) denote nighttime. ACD denotes acetaldehydes. ALD denotes the C3 and higher aldehydes. ACT and KET denote acetone and ketones. MACR and MVK denote methacrolein and methyl vinyl ketone.

To evaluate the contribution of HO_2 uptake chemistry to radical concentrations in this study, we coupled HO_2 heterogeneous uptake into the base model (RACM2-LIM1) and conducted three sensitivity experiments, as shown in R1 and Eq. (1).

HO_2 + aerosol → products R1

$$k_{HO_2+\text{aerosol}} = \frac{\gamma * \text{ASA} * \nu_{HO_2}}{4} \quad (1)$$

where ASA [μm^2 cm^{-3}], which represents the aerosol surface area concentration, can be estimated by multiplying the mass concentration of $PM_{2.5}$ [μg m^{-3}] by 20 here because there were no direct ASA observations in this campaign (Chen et al., 2019; Wang et al., 2017). ν_{HO_2}, which can be calculated by Eq. (2), refers to the mean molecular velocity of HO_2 with a unit of cm s^{-1}.

$$\nu_{HO_2} = \sqrt{\frac{8 * R * T}{0.033 * \Pi}} \quad (2)$$

where T [K] and R [J mol^{-1} K^{-1}] denote the ambient temperature and gas constant. γ, the HO_2 effective uptake coefficient, parameterizes the influence of some processes (Tan et al., 2020). γ varies in the highly uncertain range of 0-1 (Song et al., 2022), and is the most critical parameters to impact HO_2 uptake chemistry. Only several observations of γ have been reported (Taketani et al., 2012; Zhou et al., 2021; Zhou et al., 2020). The measured γ at the Mt. Tai site and Mt. Mang site were 0.13-0.34 and 0.09-0.40, respectively (Taketani et al., 2012). The averaged value of the measured γ was 0.24 in Kyoto, Japan in summer 2018 (Zhou et al., 2020). Zhou et al. (2021) reported the lower-limit values for median and average values of the measured γ were 0.19 and 0.23±0.21 in Yokohama, Japan in summer 2019. Additionally, Li et al. (2018) set 0.2 as the value of γ in the model, and Tan et al. (2020) calculated the γ of 0.08±0.13 by the analysis of the measured radical budget in Wangdu.

Herein, we applied the two γ (0.2 and 0.08), which have been used in the model, to evaluate the impact of HO_2 uptake on radical concentrations. The modeled HO_2^* cannot match well with the observations when a γ of 0.08 or 0.2 was set in the model. As the γ increased to approximately 0.3, good agreement between the modeled and observed HO_2^* concentration was achieved, demonstrating that the significant heterogeneous uptake might exist in this campaign.

It is noted that the estimated strong influence is speculative because of the uncertainties of measurements and simulations. Overall, the γ evaluated in this study was comparable with those observed at the Mt. Tai and Mt. Mang in China, and Kyoto and Yokohama in Japan.

12. Page 8, line 193. It is worth mentioning where the study (Stevens et al. 1997) took place and add more information.

Reply:

The campaign reported by Stevens et al. (1997) was conducted at Idaho Hill, Colorado, during August and September in 1993. The experimental site was located in the remote mountains, with a wide range of chemical conditions to study the kinetics of the photochemistry of radicals. This study reported two major conclusions, one was that the HO_2/OH ratios were higher in clean environments than those in polluted environments, and the other was that the measured HO_2/OH ratios agreed well with predictions under polluted environments, and they were lower than predicted values under clean environments.

13. Page 8, lines 193-194. I did not understand what the authors meant with the sentence "The comparison of the measured HO_2/OH ratio…".

Reply:

Stevens et al. (1997) reported that the agreement between the calculated and measured HO_2/OH ratio was related to several possible explanations, including the HO_2 heterogeneous reactions, instrument and/or calibration error in the measurement of radicals, or problems with the chemical oxidation mechanism. Thus, it was inaccurate to justify the environmental conditions (clean or polluted) according to the agreement of the measured and calculated HO_2/OH ratio.

Additionally, the measured HO_2/OH cannot be obtained in this study because the observed HO_2 concentrations include the true HO_2 concentrations and the interference of RO_2 radicals.

Therefore, we revised the description of HO_2/OH ratios in Section 3.2.

Revision:

The high modeled HO_2/OH ratio around noontime (11:00-15:00), which was about 138, was found in this campaign, which was higher than those in the Backgarden and Chengdu sites (Hofzumahaus et al., 2009; Yang et al., 2021). High HO_2/OH ratio is normally found only in clean air at low concentrations of Nox (Hofzumahaus et al., 2009; Stevens et al., 1997).

14. Page 10, line 232. The unknown OH source NEEDS TO explain.

Reply

To further explain the unknown OH source, we compared the environmental condition under the different NO intervals in Fig. 5 in Section 4.2.1 and Table S4 in the Supplementary Information. Besides, we explored the contribution of isoprene oxidation chemistry on missing OH source in Section 4.2.2.

Revision

(1) Section 4.2.1:

To further explore the influencing factors of OH underestimation, we presented the speciation VOCs reactivity under the different NO intervals, as shown in Fig. 5 and Table S4 in the Supplementary Information. The isoprene reactivity and total OVOCs reactivity (the sum of HCHO, ACD, ACT, ALD, KET, MACR, MVK and the modeled OVOCs) increased with the decrease of NO concentrations, while the anthropogenic VOCs reactivity (alkanes, alkenes and aromatics) was higher in high NO regime. Additionally, the O_3 concentration in low NO regime was significantly higher than those in high NO regime, and the temperature was slightly higher in low NO regime, demonstrating the photochemistry was more active in low NO regime in this campaign. Overall, the photochemistry and composition of VOCs reactivity, especially the isoprene and OVOCs species (mainly ACD, ACT and the modeled OVOCs), might closely impact the missing OH sources.

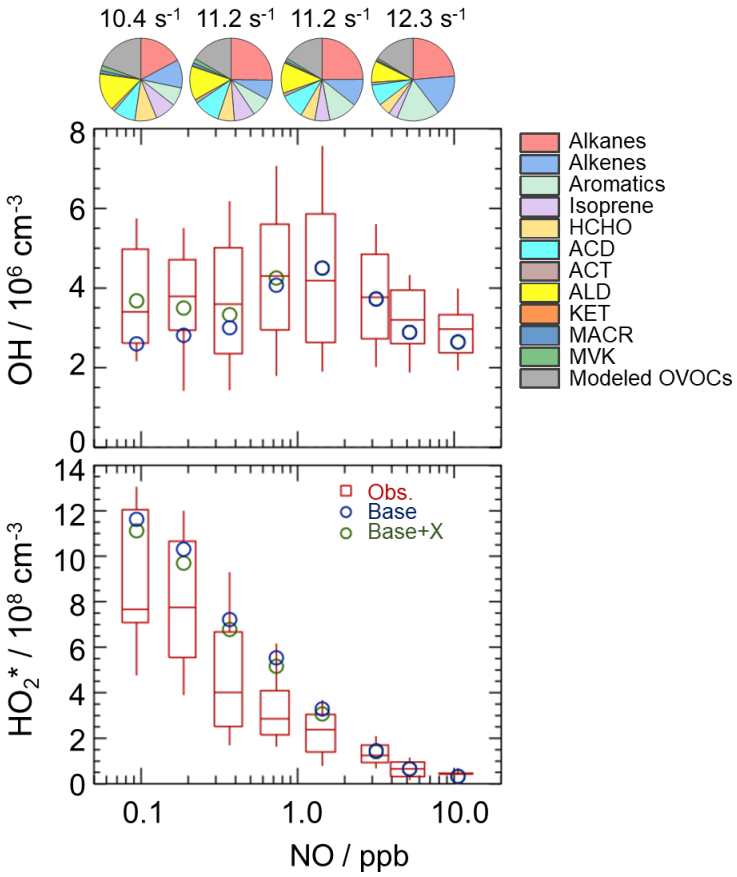

Figure 5: NO dependence of OH and HO_2^* radicals. The red box-whisker plots give the 10%, 25%, median, 75%, and 90% of the HOx observations. The blue circles show the median values of the HOx simulations by the base model, and the green circles show the HOx simulations by the model with X mechanism. Total VOCs reactivity and their organic speciation are presented by pie charts at the different NO intervals at the top. Only daytime values and NO concentration above the detection limit of the instrument were chosen. ACD and ACT denote acetaldehyde and acetone, respectively. ALD denotes the C3 and higher aldehydes. KET denotes ketones. MACR and MVK, which are both the isoprene oxidation products, denote methacrolein and methyl vinyl ketone, respectively.

(2) The median values of meteorological and chemical parameters during the daytime at the different NO intervals was added in Table S4 in the Supplementary Information:

Table S4: The median values of meteorological and chemical parameters during the daytime at the different NO intervals.

parameters	**NO interval (< 0.2 ppb)**	**NO interval (0.2-0.6 ppb)**	**NO interval (0.6-2 ppb)**	**NO interval (> 2 ppb)**
Temperature / K	301.4	300.8	299.1	297.9
$j(O^1D)$ / 10^{-6} s^{-1}	4.7	8.9	8.2	7.4
O_3 concentration / ppb	71.7	55.1	39.6	16.9
Alkanes reactivity / s^{-1}	2.2	3.4	3.3	3.5
Alkenes reactivity / s^{-1}	1.4	1.0	1.4	2.3
Aromatics reactivity / s^{-1}	0.9	1.0	1.5	2.4

Isoprene reactivity / s^{-1}	1.1	1.1	0.8	0.5
HCHO reactivity / s^{-1}	1.1	0.9	0.8	0.7
ACD reactivity / s^{-1}	1.1	1.4	1.3	1.2
ACT reactivity / s^{-1}	0.2	0.2	0.2	0.2
ALD reactivity / s^{-1}	1.9	1.8	1.6	1.2
KET reactivity / s^{-1}	0.0	0.0	0.0	0.0
MACR reactivity / s^{-1}	0.2	0.2	0.1	0.1
MVK reactivity / s^{-1}	0.3	0.2	0.1	0.1
Modeled OVOCs reactivity / s^{-1}	2.5	2.2	2.2	2.4
Alkanes concentration / ppb	15.0	16.8	19.0	24.6
Alkenes concentration / ppb	1.6	1.6	2.0	3.4
Aromatics concentration / ppb	3.3	3.3	4.8	7.9
Isoprene concentration / ppb	0.4	0.4	0.3	0.2
HCHO concentration / ppb	5.6	4.3	3.8	3.5
ACD concentration / ppb	3.0	3.7	3.5	3.3
ACT concentration / ppb	3.2	3.7	3.3	2.7
ALD concentration / ppb	3.8	3.6	3.2	2.5
KET concentration / ppb	0.3	0.4	0.4	0.3
MACR concentration / ppb	0.2	0.2	0.1	0.1
MVK concentration / ppb	0.5	0.5	0.3	0.2

(3) Section 4.2.2

As discussed in Section 4.2.1, isoprene and OVOCs might have potential influence on the missing OH source. RO_2 isomerization reactions have also been shown to be of importance for the atmospheric fate of RO_2 from isoprene (Peeters et al., 2009; Peeters et al., 2014). The latest isoprene isomerization mechanism, which is called LIM1, has been coupled into our current base model. However, LIM1 mechanism was not included in the OH experimental budget which was conducted with the observations constrained, as shown in Section 4.1. Herein, we evaluated the contribution of LIM1 mechanism to the missing OH sources, as shown in Fig. 4 (b). LIM1 mechanism can explain approximately 7% of the missing OH sources during 10:00-16:00, when the missing OH production rate and the OH production rate derived from LIM1 were 2.47 ppb h^{-1} and 0.17 ppb h^{-1}, respectively.

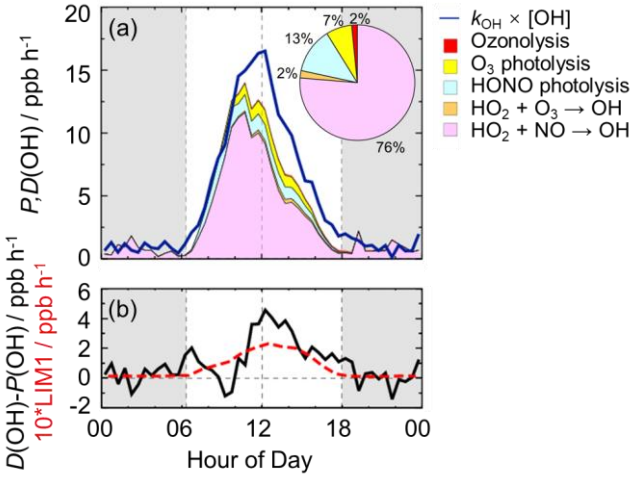

Figure 4: (a) The diurnal profiles of OH production and destruction rates and the proportions of different known sources in the calculated production rate during the daytime. The blue line denotes the OH destruction rate, and the colored areas denote the calculated OH production rates from the known sources. (b) The missing OH production rate which was the discrepancy between the OH destruction and production rates, and the OH production rate which was ten times the production rate derived from LIM1 mechanism. The grey areas denote nighttime.

Additionally, prior studies also reported that OH regeneration might be achieved from the oxidation of MACR and MVK, which are the major first-generated products of isoprene (Fuchs et al., 2018; Fuchs et al., 2014). As a potential explanation for the high OH concentration, the impacts of MACR and MVK oxidation were evaluated here. The modification of MACR oxidation scheme added the H-migration reactions of MACR oxidation products (Fuchs et al., 2014). The modification of MVK oxidation scheme added the reactions of MVK oxidation products with HO_2 radicals and the H-migration reactions of MVK oxidation products (Fuchs et al., 2018). As presented in Fig. S3 in the Supplementary Information, no significant of the MACR and MVK oxidation schemes was found in this campaign.

Overall, a large part of missing OH sources was not explained by the isoprene chemistry. In the future, the impact of OVOCs species which was another potential OH source on missing OH sources need to be further evaluated.

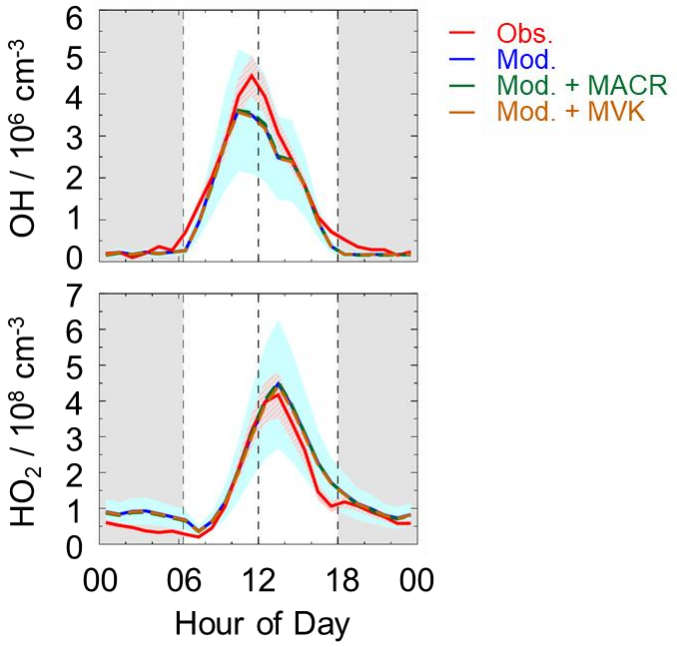

Figure S3: The diurnal profiles of the observed and modeled radical concentrations. The red and blue areas denote 1-σ uncertainties of measured and simulated radical concentrations by the base model, respectively. The green lines denote the simulations by the model with the oxidation of MACR, and the dark orange lines denote the simulations by the model with the oxidation of MVK. The grey areas denote nighttime.

15. Page 10, lines 251-252. Species other than NO played a significant role to explain the model's OH underestimation.

Reply

In the Reply to Question 14, we compared the composition of VOCs reactivity under the different NO intervals. We found the percentage of isoprene and OVOCs species (especially aldehydes and modeled OVOCs) in the total VOCs reactivity was higher in low NO regime. The contribution of isoprene and its oxidation products (MACR and MVK) to the missing OH source was evaluated. The detailed discussions were presented in the Reply to Question 14.

16. Page 13, Line 301, Table 1. AOC includes all combination of pollutants i and oxidant j (j= OH, O_3, NO_3)? As the equation (1) does not include j, this in unclear.

Reply

Yes, AOC includes all combination of pollutants (eg. VOCs, CO and CH_4) and oxidants (OH, O_3 and NO_3).

Revision

Section 2.3:

AOC includes all combination of pollutants Y and oxidants X.

17. Page 14, Figure 7c. Why different units are used for the AOC and F(O_3)? They can be both in ppb h-1 for example and should have close values.

Reply

We revised the unit of AOC to ppb h^{-1}, which is the same as the unit of O_3 formation. Additionally, we have taken the helpful third comment in your 'General comments' into account, and we added the NO dependence of $P(O_3)$, AOC and the ratio of $P(O_3)$ to AOC in Fig. 7 (b-d).

Revision

(1) Section 4.4:

As the indictor for secondary pollution, net O_3 production rate, $P(O_3)$, can be calculated from the O_3 formation rate ($F(O_3)$) and O_3 loss rate ($L(O_3)$), as shown in Eq. (3-5) (Tan et al., 2017). The diurnal profiles of the speciation $F(O_3)$ and $L(O_3)$ were shown in Fig. S5 in the Supplementary Information. The diurnal maxima of the modeled $F(O_3)$ and $L(O_3)$ were 18.9 ppb h^{-1} and 2.8 ppb h^{-1}, with the maximum $P(O_3)$ of 16.1 ppb h^{-1} at 11:00. The modeled $P(O_3)$ was comparable to that in Wangdu site in summer and much higher than that in Beijing in winter (Tan et al., 2018; Tan et al., 2017).

$$F(O_3) = k_{HO_2+NO}[HO_2][NO] + \sum_i k_{RO_2i+NO}[RO_2]_i[NO] \quad (3)$$

$$L(O_3) = \theta j(O^1D)[O_3] + k_{O_3+OH}[O_3][OH] + k_{O_3+HO_2}[O_3][HO_2] + (\sum(k^i_{alkenes+O_3}[alkenes^i]))[O_3] \quad (4)$$

$$P(O_3) = F(O_3) - L(O_3) \quad (5)$$

where θ is the fraction of O^1D from ozone photolysis that reacts with water vapor.

Herein, we presented the NO dependence of $P(O_3)$, AOC_{VOCs}, and ratio of $P(O_3)$ to AOC_{VOCs} in Fig. 7 (b-d), in which AOC_{VOCs} denotes the atmospheric oxidation capacity only from the VOCs oxidation. An upward trend $P(O_3)$ was presented with the increase of NO concentration when NO concentration was below 1 ppb, while a downward trend was shown with the increase of NO concentration when NO concentration was above 1 ppb. In terms of the NO dependence of AOC_{VOCs}, no significant variation was found, indicating VOCs oxidation was weakly impacted by NO concentrations in this campaign. Since AOC_{VOCs} can represent the VOCs oxidant rate, and thus the ratio of $P(O_3)$ to AOC_{VOCs} can reflect the yield of ozone production from VOCs oxidation. Similar to $P(O_3)$, the ratio increased with the increase of NO concentration when NO concentration was below 1 ppb. When NO concentration was above 1 ppb, the ratio decreased with the increase of NO concentration because NO_2 became the sink of OH radicals gradually. The maximum of the ratios existed when NO concentration was approximately 1 ppb, with a median of about 2, indicating the yield of ozone production from VOCs oxidation was about 2 in this study.

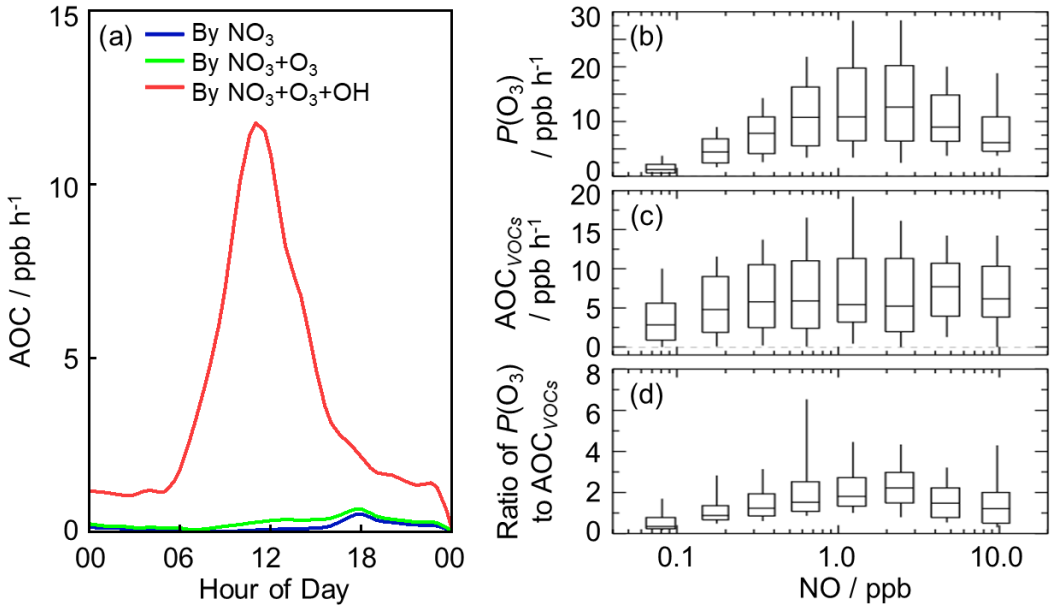

Figure 7: (a) The diurnal profiles of AOC in this campaign. (b) NO dependence of $P(O_3)$ during the daytime. (c) NO dependence of AOC_{VOCs} during the daytime, and AOC_{VOCs} denotes the atmospheric oxidation capacity only from the VOCs oxidation. (d) NO dependence of the ratio of $P(O_3)$ to AOC_{VOCs} during the daytime. The box-whisker plots in (b-d) give the 10%, 25%, median, 75%, and 90% of $P(O_3)$, AOC and the ratio of $P(O_3)$ to AOC, respectively.

(2) The diurnal profiles of $P(O_3)$, $F(O_3)$, and $L(O_3)$ were added in Figure S5 in the Supplementary Information:

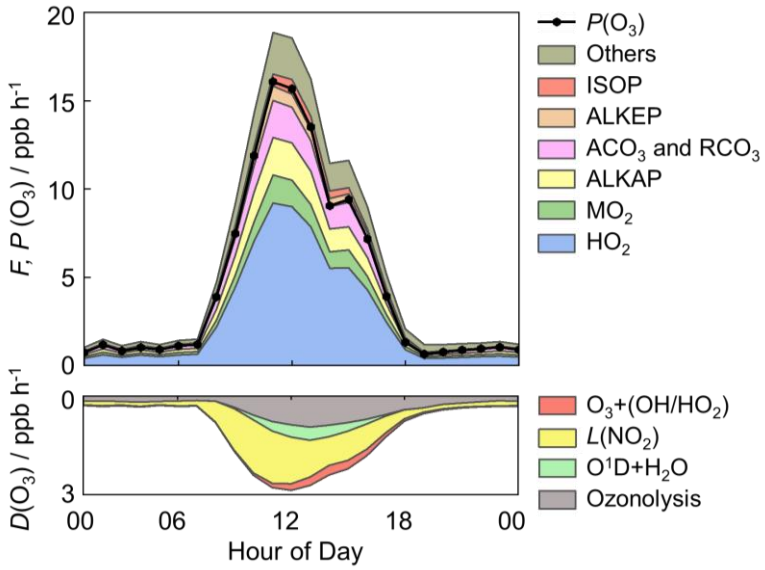

Figure S5: The diurnal profiles of $P(O_3)$, $F(O_3)$, and $L(O_3)$ in this campaign. The colored areas denote the speciation of $F(O_3)$ and $L(O_3)$ in the upper panel and lower panel, respectively. The black line denotes the $P(O_3)$, which is the discrepancy between $F(O_3)$ and $L(O_3)$. MO_2 denotes the methyl peroxy radicals. ALKAP, ALKEP and ISOP denote the RO_2 radicals derived from alkanes, alkenes and isoprene, respectively. ACO_3 denotes the acetyl peroxy radicals, and RCO_3 denotes the higher saturated acyl peroxy radicals.

18. Page 14, Line 322. Why a fixed value (9x10^-12) is used for the rate constants of the RO_2 + NO reactions? They should be variable in RACM depending of R and therefore these values should be used.

Reply

Thanks for your helpful suggestions. As shown in the Reply to Question 17, we revised the equations of O_3 formation and loss rates, and we re-calculated the O_3 formation rate, O_3 loss rate and net O_3 production rate based on the reactions of specific RO_2 speciation and NO.

19. Page 15, lines 351-352. Rewording is necessary.

Reply

As shown in the Reply to Question 11, we revised this sentence in the manuscript.

Revision

As for HO_2 radicals, the overestimation of HO_2^* concentration was found, indicating that HO_2 heterogeneous uptake might make a significant role in HO_2 sinks.

20. Page 16, line 362. What are the gradients here?

Reply

As shown in the Reply to Question 17, we revised the contents of Section 4.4. Thus, the description of AOC in Section 5 was revised as follows.

Revision

In this campaign, AOC exhibited well-defined diurnal patterns, with a peak of 11.8 ppb h^{-1}. As expected, OH was the dominant oxidant accounting for 95.7% of the total AOC during the daytime. O_3 and NO_3 contributed 2.9% and 1.4% to total AOC during the daytime, respectively. The ratio of $P(O_3)$ to AOC_{VOCs} trended to increase and then decrease as NO concentration increased, demonstrating the non-linear relationship between O_3 production and VOCs oxidation. The maximum of the ratios existed when NO concentration was approximately 1 ppb, with a median of about 2, indicating that the yield of ozone production from VOCs oxidation was about 2 in this campaign.

21. Page 16, line 363. makes the quantification of $F(O_3)$ achieved – rewording is necessary.

Reply

As shown in the Reply to Question 17 and Question 20, the description of AOC in Section 5 was revised as follows.

Revision

In this campaign, AOC exhibited well-defined diurnal patterns, with a peak of 11.8 ppb h^{-1}. As expected, OH was the dominant oxidant accounting for 95.7% of the total AOC during the daytime. O_3 and NO_3 contributed 2.9% and 1.4% to total AOC during the daytime, respectively. The ratio of $P(O_3)$ to AOC_{VOCs} trended to increase and then decrease as NO concentration increased, demonstrating the non-linear relationship between O_3 production and VOCs

oxidation. The maximum of the ratios existed when NO concentration was approximately 1 ppb, with a median of about 2, indicating that the yield of ozone production from VOCs oxidation was about 2 in this campaign.

References

Chen, X., Wang, H., Liu, Y., Su, R., Wang, H., Lou, S., and Lu, K.: Spatial characteristics of the nighttime oxidation capacity in the Yangtze River Delta, China, Atmospheric Environment, 208, 150-157, 10.1016/j.atmosenv.2019.04.012, 2019.

Fan, S., Wang, A., Fan, Q., Liu, J., and Wang, B.: ATMOSPHERIC BOUNDARY LAYER CONCEPT MODEL OF THE PEARL RIVER DELTA AND ITS APPLICATION, Journal of Tropical Meteorology, 21, 286-292, 2005.

Fuchs, H., Holland, F., and Hofzumahaus, A.: Measurement of tropospheric RO2 and HO2 radicals by a laser-induced fluorescence instrument, Review of Scientific Instruments, 79, 10.1063/1.2968712, 2008.

Fuchs, H., Bohn, B., Hofzumahaus, A., Holland, F., Lu, K. D., Nehr, S., Rohrer, F., and Wahner, A.: Detection of HO2 by laser-induced fluorescence: calibration and interferences from RO2 radicals, Atmospheric Measurement Techniques, 4, 1209-1225, 10.5194/amt-4-1209-2011, 2011.

Fuchs, H., Acir, I. H., Bohn, B., Brauers, T., Dorn, H. P., Häseler, R., Hofzumahaus, A., Holland, F., Kaminski, M., Li, X., Lu, K., Lutz, A., Nehr, S., Rohrer, F., Tillmann, R., Wegener, R., and Wahner, A.: OH regeneration from methacrolein oxidation investigated in the atmosphere simulation chamber SAPHIR, Atmos. Chem. Phys., 14, 7895-7908, 10.5194/acp-14-7895-2014, 2014.

Fuchs, H., Albrecht, S., Acir, I.-H., Bohn, B., Breitenlechner, M., Dorn, H.-P., Gkatzelis, G. I., Hofzumahaus, A., Holland, F., Kaminski, M., Keutsch, F. N., Novelli, A., Reimer, D., Rohrer, F., Tillmann, R., Vereecken, L., Wegener, R., Zaytsev, A., Kiendler-Scharr, A., and Wahner, A.: Investigation of the oxidation of methyl vinyl ketone (MVK) by OH radicals in the atmospheric simulation chamber SAPHIR, Atmospheric Chemistry and Physics, 18, 8001-8016, 10.5194/acp-18-8001-2018, 2018.

Fuchs, H., Tan, Z., Lu, K., Bohn, B., Broch, S., Brown, S. S., Dong, H., Gomm, S., Haeseler, R., He, L., Hofzumahaus, A., Holland, F., Li, X., Liu, Y., Lu, S., Min, K.-E., Rohrer, F., Shao, M., Wang, B., Wang, M., Wu, Y., Zeng, L., Zhang, Y., Wahner, A., and Zhang, Y.: OH reactivity at a rural site (Wangdu) in the North China Plain: contributions from OH reactants and experimental OH budget, Atmospheric Chemistry and Physics, 17, 645-661, 10.5194/acp-17-645-2017, 2017.

Gao, M., Li, H., Li, Y., Wei, J., Sun, Y., He, L., and Huang, X.: Source characteristics of water-soluble organic matters in PM_(2.5) in the winter of Shenzhen, China Environmental Science, 38, 4017-4022, 2018.

Heard, D. E. and Pilling, M. J.: Measurement of OH and HO2 in the troposphere, Chemical Reviews, 103, 5163-5198, 10.1021/cr020522s, 2003.

Hofzumahaus, A., Aschmutat, U., Hessling, M., Holland, F., and Ehhalt, D. H.: The measurement of tropospheric OH radicals by laser-induced fluorescence spectroscopy during the POPCORN field campaign, Geophysical Research Letters, 23, 2541-2544, 10.1029/96gl02205, 1996.

Hofzumahaus, A., Rohrer, F., Lu, K., Bohn, B., Brauers, T., Chang, C.-C., Fuchs, H., Holland, F., Kita, K., Kondo, Y., Li, X., Lou, S., Shao, M., Zeng, L., Wahner, A., and Zhang, Y.: Amplified Trace Gas Removal in the Troposphere, Science, 324, 1702-1704, 10.1126/science.1164566, 2009.

Holland, F., Hessling, M., and Hofzumahaus, A.: IN-SITU MEASUREMENT OF TROPOSPHERIC OH RADICALS BY LASER-INDUCED FLUORESCENCE - A DESCRIPTION OF THE KFA INSTRUMENT, Journal of the Atmospheric Sciences, 52, 3393-3401, 10.1175/1520-

0469(1995)052<3393:Ismoto>2.0.Co;2, 1995.
Huang, X.-F., Sun, T.-L., Zeng, L.-W., Yu, G.-H., and Luan, S.-J.: Black carbon aerosol characterization in a coastal city in South China using a single particle soot photometer, Atmospheric Environment, 51, 21-28, https://doi.org/10.1016/j.atmosenv.2012.01.056, 2012a.
Huang, X.-F., Chen, D.-L., Lan, Z.-J., Feng, N., He, L.-Y., Yu, G.-H., and Luan, S.-J.: Characterization of organic aerosol in fine particles in a mega-city of South China: Molecular composition, seasonal variation, and size distribution, Atmospheric Research, 114-115, 28-37, https://doi.org/10.1016/j.atmosres.2012.05.019, 2012b.
Liu, S., Li, X., Shen, X., Zeng, L., Huang, X., Zhu, B., Lin, L., and Lou, S.: Measurement and partition analysis of atmospheric OH reactivity in autumn in Shenzhen, Acta Scientiae Circumstantiae, 39, 3600-3610, 2019.
Lou, S., Holland, F., Rohrer, F., Lu, K., Bohn, B., Brauers, T., Chang, C. C., Fuchs, H., Haeseler, R., Kita, K., Kondo, Y., Li, X., Shao, M., Zeng, L., Wahner, A., Zhang, Y., Wang, W., and Hofzumahaus, A.: Atmospheric OH reactivities in the Pearl River Delta - China in summer 2006: measurement and model results, Atmospheric Chemistry and Physics, 10, 11243-11260, 10.5194/acp-10-11243-2010, 2010.
Lu, K. D., Hofzumahaus, A., Holland, F., Bohn, B., Brauers, T., Fuchs, H., Hu, M., Haeseler, R., Kita, K., Kondo, Y., Li, X., Lou, S. R., Oebel, A., Shao, M., Zeng, L. M., Wahner, A., Zhu, T., Zhang, Y. H., and Rohrer, F.: Missing OH source in a suburban environment near Beijing: observed and modelled OH and HO2 concentrations in summer 2006, Atmospheric Chemistry and Physics, 13, 1057-1080, 10.5194/acp-13-1057-2013, 2013.
Lu, K. D., Rohrer, F., Holland, F., Fuchs, H., Bohn, B., Brauers, T., Chang, C. C., Haeseler, R., Hu, M., Kita, K., Kondo, Y., Li, X., Lou, S. R., Nehr, S., Shao, M., Zeng, L. M., Wahner, A., Zhang, Y. H., and Hofzumahaus, A.: Observation and modelling of OH and HO2 concentrations in the Pearl River Delta 2006: a missing OH source in a VOC rich atmosphere, Atmospheric Chemistry and Physics, 12, 1541-1569, 10.5194/acp-12-1541-2012, 2012.
Peeters, J., Nguyen, T. L., and Vereecken, L.: HOx radical regeneration in the oxidation of isoprene, Physical Chemistry Chemical Physics, 11, 5935-5939, 10.1039/b908511d, 2009.
Peeters, J., Muller, J.-F., Stavrakou, T., and Vinh Son, N.: Hydroxyl Radical Recycling in Isoprene Oxidation Driven by Hydrogen Bonding and Hydrogen Tunneling: The Upgraded LIM1 Mechanism, Journal of Physical Chemistry A, 118, 8625-8643, 10.1021/jp5033146, 2014.
Song, H., Lu, K., Dong, H., Tan, Z., Chen, S., Zeng, L., and Zhang, Y.: Reduced Aerosol Uptake of Hydroperoxyl Radical May Increase the Sensitivity of Ozone Production to Volatile Organic Compounds, Environmental Science & Technology Letters, 9, 22-29, 10.1021/acs.estlett.1c00893, 2022.
Stevens, P. S., Mather, J. H., Brune, W. H., Eisele, F., Tanner, D., Jefferson, A., Cantrell, C., Shetter, R., Sewall, S., Fried, A., Henry, B., Williams, E., Baumann, K., Goldan, P., and Kuster, W.: HO2/OH and RO(2)/HO2 ratios during the Tropospheric OH Photochemistry Experiment: Measurement and theory, Journal of Geophysical Research-Atmospheres, 102, 6379-6391, 10.1029/96jd01704, 1997.
Taketani, F., Kanaya, Y., Pochanart, P., Liu, Y., Li, J., Okuzawa, K., Kawamura, K., Wang, Z., and Akimoto, H.: Measurement of overall uptake coefficients for HO2 radicals by aerosol particles sampled from ambient air at Mts. Tai and Mang (China), Atmospheric Chemistry and Physics, 12, 11907-11916, 10.5194/acp-12-11907-2012, 2012.
Tan, Z., Lu, K., Hofzumahaus, A., Fuchs, H., Bohn, B., Holland, F., Liu, Y., Rohrer, F., Shao, M., Sun, K., Wu, Y., Zeng, L., Zhang, Y., Zou, Q., Kiendler-Scharr, A., Wahner, A., and Zhang, Y.: Experimental budgets of OH, HO2, and RO2 radicals and implications for ozone formation in the Pearl River Delta in

China 2014, Atmospheric Chemistry and Physics, 19, 7129-7150, 10.5194/acp-19-7129-2019, 2019.
Tan, Z., Hofzumahaus, A., Lu, K., Brown, S. S., Holland, F., Huey, L. G., Kiendler-Scharr, A., Li, X., Liu, X., Ma, N., Min, K.-E., Rohrer, F., Shao, M., Wahner, A., Wang, Y., Wiedensohler, A., Wu, Y., Wu, Z., Zeng, L., Zhang, Y., and Fuchs, H.: No Evidence for a Significant Impact of Heterogeneous Chemistry on Radical Concentrations in the North China Plain in Summer 2014, Environmental Science & Technology, 54, 5973-5979, 10.1021/acs.est.0c00525, 2020.
Tan, Z., Fuchs, H., Lu, K., Hofzumahaus, A., Bohn, B., Broch, S., Dong, H., Gomm, S., Haeseler, R., He, L., Holland, F., Li, X., Liu, Y., Lu, S., Rohrer, F., Shao, M., Wang, B., Wang, M., Wu, Y., Zeng, L., Zhang, Y., Wahner, A., and Zhang, Y.: Radical chemistry at a rural site (Wangdu) in the North China Plain: observation and model calculations of OH, HO2 and RO2 radicals, Atmospheric Chemistry and Physics, 17, 663-690, 10.5194/acp-17-663-2017, 2017.
Tan, Z., Rohrer, F., Lu, K., Ma, X., Bohn, B., Broch, S., Dong, H., Fuchs, H., Gkatzelis, G. I., Hofzumahaus, A., Holland, F., Li, X., Liu, Y., Liu, Y., Novelli, A., Shao, M., Wang, H., Wu, Y., Zeng, L., Hu, M., Kiendler-Scharr, A., Wahner, A., and Zhang, Y.: Wintertime photochemistry in Beijing: observations of ROx radical concentrations in the North China Plain during the BEST-ONE campaign, Atmospheric Chemistry and Physics, 18, 12391-12411, 10.5194/acp-18-12391-2018, 2018.
Wang, X., Wang, H., Xue, L., Wang, T., Wang, L., Gu, R., Wang, W., Tham, Y. J., Wang, Z., Yang, L., Chen, J., and Wang, W.: Observations of N2O5 and ClNO2 at a polluted urban surface site in North China: High N2O5 uptake coefficients and low ClNO2 product yields, Atmospheric Environment, 156, 125-134, 10.1016/j.atmosenv.2017.02.035, 2017.
Whalley, L. K., Slater, E. J., Woodward-Massey, R., Ye, C., Lee, J. D., Squires, F., Hopkins, J. R., Dunmore, R. E., Shaw, M., Hamilton, J. F., Lewis, A. C., Mehra, A., Worrall, S. D., Bacak, A., Bannan, T. J., Coe, H., Percival, C. J., Ouyang, B., Jones, R. L., Crilley, L. R., Kramer, L. J., Bloss, W. J., Vu, T., Kotthaus, S., Grimmond, S., Sun, Y., Xu, W., Yue, S., Ren, L., Acton, W. J. F., Hewitt, C. N., Wang, X., Fu, P., and Heard, D. E.: Evaluating the sensitivity of radical chemistry and ozone formation to ambient VOCs and NOx in Beijing, Atmospheric Chemistry and Physics, 21, 2125-2147, 10.5194/acp-21-2125-2021, 2021.
Yang, X., Lu, K., Ma, X., Liu, Y., Wang, H., Hu, R., Li, X., Lou, S., Chen, S., Dong, H., Wang, F., Wang, Y., Zhang, G., Li, S., Yang, S., Yang, Y., Kuang, C., Tan, Z., Chen, X., Qiu, P., Zeng, L., Xie, P., and Zhang, Y.: Observations and modeling of OH and HO2 radicals in Chengdu, China in summer 2019, The Science of the total environment, 772, 144829-144829, 10.1016/j.scitotenv.2020.144829, 2021.
Zhang, Y. H., Hu, M., Zhong, L. J., Wiedensohler, A., Liu, S. C., Andreae, M. O., Wang, W., and Fan, S. J.: Regional Integrated Experiments on Air Quality over Pearl River Delta 2004 (PRIDE-PRD2004): Overview, Atmospheric Environment, 42, 6157-6173, 10.1016/j.atmosenv.2008.03.025, 2008.
Zhou, J., Murano, K., Kohno, N., Sakamoto, Y., and Kajii, Y.: Real-time quantification of the total HO2 reactivity of ambient air and HO2 uptake kinetics onto ambient aerosols in Kyoto (Japan), Atmospheric Environment, 223, 10.1016/j.atmosenv.2020.117189, 2020.
Zhou, J., Sato, K., Bai, Y., Fukusaki, Y., Kousa, Y., Ramasamy, S., Takami, A., Yoshino, A., Nakayama, T., Sadanaga, Y., Nakashima, Y., Li, J., Murano, K., Kohno, N., Sakamoto, Y., and Kajii, Y.: Kinetics and impacting factors of HO2 uptake onto submicron atmospheric aerosols during the 2019 Air QUAlity Study (AQUAS) in Yokohama, Japan, Atmospheric Chemistry and Physics, 21, 12243-12260, 10.5194/acp-21-12243-2021, 2021.

Response to Reviewer comment #3:

General comments:

This paper presents measurements of OH and HO_2 radicals during the STORM campaign in the Pearl River Delta and compare their measurements to model predictions. The authors conclude that the model underestimates the measured OH concentration but can reproduce the measured HO2 concentrations. The authors propose that the "X" mechanism can explain the discrepancy, similar to that proposed in previous studies. The proposed mechanism involves an unmeasured species "X" that converts RO_2 to HO_2 and HO_2 to OH similar to NO. The authors conclude that a mixing ratio of "X" equivalent to 0.1 ppb of NO is needed to bring the measured OH concentrations into agreement with the measurements.

However, it is not clear that their measurements support their conclusion that the model significantly underestimates the measured concentrations, as it appears that the model agrees with the measurements to within the uncertainty of the technique. This is in contrast to the previous measurements highlighted in the paper, where the discrepancy between models and measurements were found to be much greater, such as the factor of 3-5 found by Hofzumahaus et al. (2009). While the addition of the X mechanism does improve the agreement with the measurements, there is no discussion as to why the measurements reported here are in better agreement with the model compared to the previous measurements discussed in the paper. The paper would benefit from an expanded discussion of the measurement-model agreement taking the uncertainties associate with both into account. In addition, the paper would benefit from an expanded discussion of a comparison of their results with the previous measurements mentioned in the manuscript, especially the difference between their measurements and those at the Backgarden and Heshan sites in the PRD (Hofzumahaus et al., 2009; Tan et al., 2019). Such a discussion could provide more information about the source of the model-measurement discrepancies at all these sites.

The measurements of OH and HO_2 appear to be high quality and are of interest to the atmospheric chemistry community. In addition to addressing the major comment described above, I believe the paper would be publishable after the authors also address the following in a revised manuscript.

Reply

Thanks for your critical comments and suggestions concerning our manuscript. We have studied all the comments which were helpful for revising and improving our manuscript. We have made corrections which we hope meet with approval. Below are our responses to the specific comments, highlighted in blue, with changes to the manuscript highlighted in green.

Specific comments:

1. The authors state that the base model agrees with the measurements to within the uncertainties of the measurements and the model (line 177), but then states that the model underestimates the measurements after 10 am when NO decreases. However, based on the information provided in Figure 3a, it appears that the model still agrees with the measurements to within the combined uncertainty of both the model and the measurements. This should be clarified. Addition of uncertainty estimates in Figure 3 would help to illustrate the agreement.

Reply

We recheck the data (details in the Reply to Question 4) and added the uncertainty of radical concentrations in fig. 3 as your suggestions. The description of the comparison between the observed and modeled radical concentrations was revised in Section 3.2.

Revision

Section 3.2:

The observed and modeled OH concentrations agreed within their 1-σ uncertainties of measurement and simulation (11% and 40%). However, when the NO mixing ratio (Fig. 2) dropped from 10:00 gradually, a systematic difference existed, with the observed OH concentration being about 1×10^6 cm^{-3} higher than the modeled OH concentration.

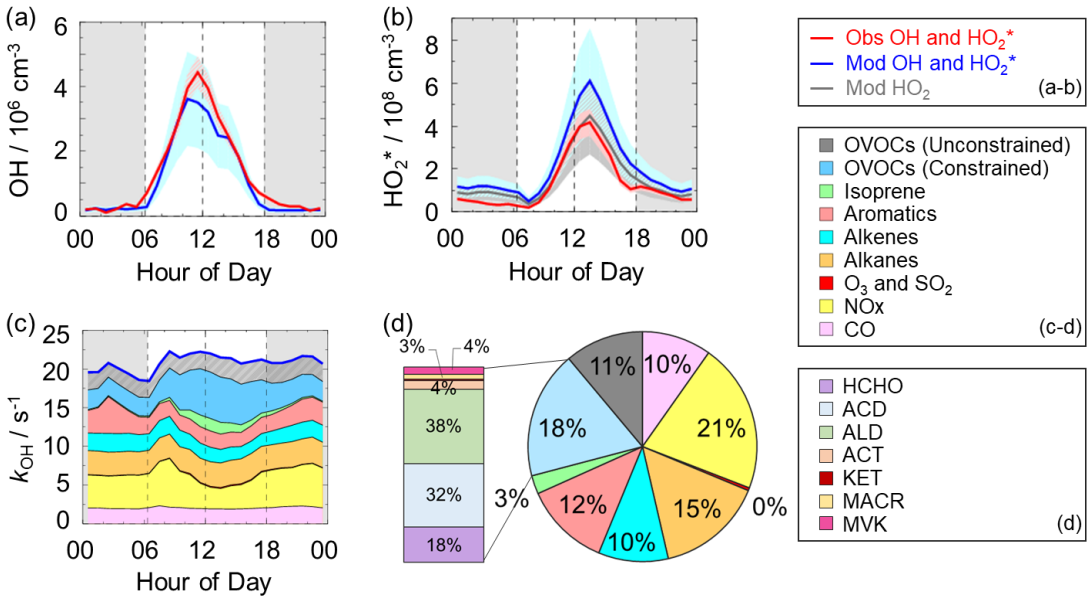

Figure 3: (a-b) The diurnal profiles of the observed and modeled OH, HO_2^* and HO_2 concentrations. (c) The diurnal profiles of the modeled k_{OH}. (d) The composition of the modeled k_{OH}. The red areas in (a-b) denote 1-σ uncertainties of the observed OH and HO_2^* concentrations. The blue areas in (a-b) denote 1-σ uncertainties of the modeled OH and HO_2^* concentrations, and the grey area in (b) denotes 1-σ uncertainties of the modeled HO_2 concentrations. The grey areas in (a-c) denote nighttime. ACD denotes acetaldehydes. ALD denotes the C3 and higher aldehydes. ACT and KET denote acetone and ketones. MACR and MVK denote methacrolein and methyl vinyl ketone.

2. Similarly, the base model predictions at low NO shown in Figure 5, although lower than the median measurements, appear to be within the combined uncertainty of model and measurements. The authors should quantify the discrepancy between the measurements and the model at each NO bin and reassess whether there is significant disagreement at low NO.

Reply

Thanks for your suggestions. The box-whisker plots in Fig. 5 denote the 10%, 25%, median, 75%, and 90% of HOx observations during the whole campaign rather than the 1-σ uncertainty of HOx observations. Herein, we compared the daily median of the observed and modeled OH concentrations with 1-σ uncertainty under the low NO intervals during the noontime (< 0.2 ppb, 0.2-0.6 ppb) in the following figure. The medium modeled OH concentrations were lower than the medium observed concentrations on most days. When we considered the combined uncertainty of OH observations (11%) and simulation (40%), the modeled OH concentrations were still lower than the OH observations on several days, especially when NO concentration was below 0.2 ppb.

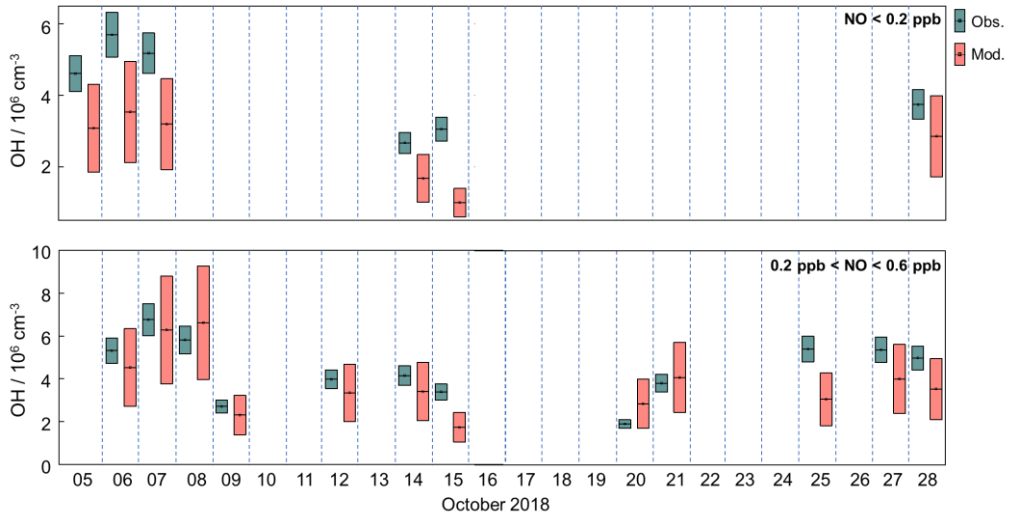

Figure: The daily median of the observed and modeled OH concentration with 1-σ uncertainty under the low NO intervals (< 0.2 ppb, 0.2-0.6 ppb) during the noontime.

Additionally, we further explored the composition of VOCs reactivity under the different NO intervals, as shown in the revised Fig. 5.

Revision

(1) Section 4.2.1:

To further explore the influencing factors of OH underestimation, we presented the speciation VOCs reactivity under the different NO intervals, as shown in Fig. 5 and Table S4 in the Supplementary Information. The isoprene reactivity and total OVOCs reactivity (the sum of HCHO, ACD, ACT, ALD, KET, MACR, MVK and the modeled OVOCs) increased with the decrease of NO concentrations, while the anthropogenic VOCs reactivity (alkanes, alkenes and aromatics) was higher in high NO regime. Additionally, the O_3 concentration in low NO regime was significantly higher than those in high NO regime, and the temperature was slightly higher in low NO regime, demonstrating the photochemistry was more active in low NO regime in

this campaign. Overall, the photochemistry and composition of VOCs reactivity, especially the isoprene and OVOCs species (mainly ACD, ACT and the modeled OVOCs), might closely impact the missing OH sources.

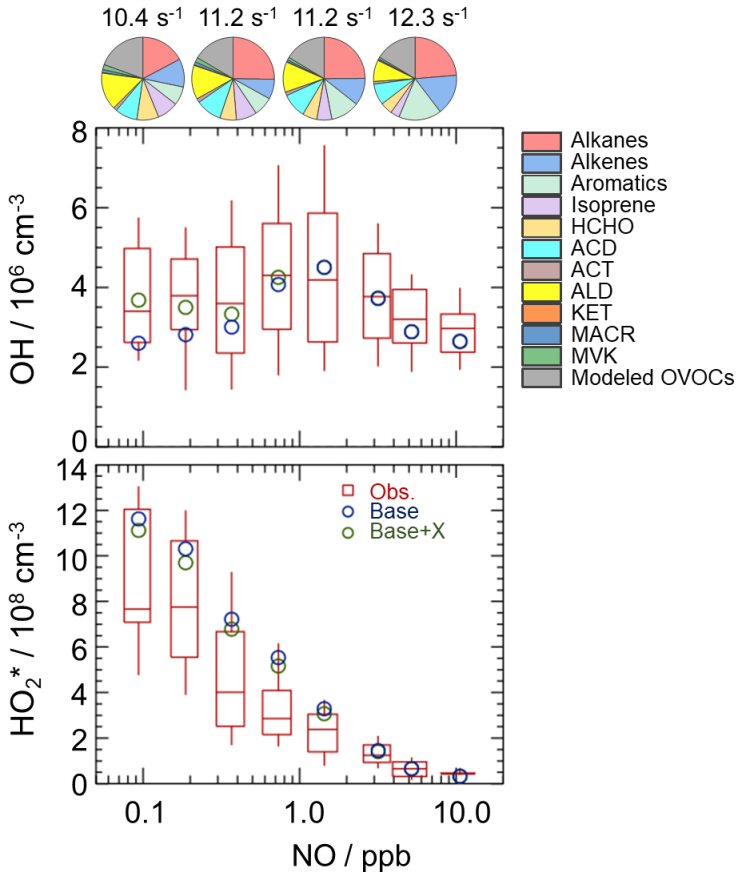

Figure 5: NO dependence of OH and HO_2^* radicals. The red box-whisker plots give the 10%, 25%, median, 75%, and 90% of the HOx observations. The blue circles show the median values of the HOx simulations by the base model, and the green circles show the HOx simulations by the model with X mechanism. Total VOCs reactivities and their organic speciation are presented by pie charts at the different NO intervals at the top. Only daytime values and NO concentration above the detection limit of the instrument were chosen. ACD and ACT denote acetaldehyde and acetone, respectively. ALD denotes the C3 and higher aldehydes. KET denotes ketones. MACR and MVK, which are both the isoprene oxidation products, denote methacrolein and methyl vinyl ketone, respectively.

(2) The median values of meteorological and chemical parameters during the daytime at the different NO intervals were added in Table S4 in the Supplementary Information:

Table S4: The median values of meteorological and chemical parameters during the daytime at the different NO intervals.

parameters	NO interval (< 0.2 ppb)	NO interval (0.2-0.6 ppb)	NO interval (0.6-2 ppb)	NO interval (> 2 ppb)
Temperature / K	301.4	300.8	299.1	297.9
$j(O^1D)$ / 10^{-6} s^{-1}	4.7	8.9	8.2	7.4
O_3 concentration / ppb	71.7	55.1	39.6	16.9

Alkanes reactivity / s^{-1}	2.2	3.4	3.3	3.5
Alkenes reactivity / s^{-1}	1.4	1.0	1.4	2.3
Aromatics reactivity / s^{-1}	0.9	1.0	1.5	2.4
Isoprene reactivity / s^{-1}	1.1	1.1	0.8	0.5
HCHO reactivity / s^{-1}	1.1	0.9	0.8	0.7
ACD reactivity / s^{-1}	1.1	1.4	1.3	1.2
ACT reactivity / s^{-1}	0.2	0.2	0.2	0.2
ALD reactivity / s^{-1}	1.9	1.8	1.6	1.2
KET reactivity / s^{-1}	0.0	0.0	0.0	0.0
MACR reactivity / s^{-1}	0.2	0.2	0.1	0.1
MVK reactivity / s^{-1}	0.3	0.2	0.1	0.1
Modeled OVOCs reactivity / s^{-1}	2.5	2.2	2.2	2.4
Alkanes concentration / ppb	15.0	16.8	19.0	24.6
Alkenes concentration / ppb	1.6	1.6	2.0	3.4
Aromatics concentration / ppb	3.3	3.3	4.8	7.9
Isoprene concentration / ppb	0.4	0.4	0.3	0.2
HCHO concentration / ppb	5.6	4.3	3.8	3.5
ACD concentration / ppb	3.0	3.7	3.5	3.3
ACT concentration / ppb	3.2	3.7	3.3	2.7
ALD concentration / ppb	3.8	3.6	3.2	2.5
KET concentration / ppb	0.3	0.4	0.4	0.3
MACR concentration / ppb	0.2	0.2	0.1	0.1
MVK concentration / ppb	0.5	0.5	0.3	0.2

3. The analysis of the OH measurements assumes that there are no interferences associated with the LIF-FAGE measurements. However, there is no discussion of whether the authors tested for unknown interferences with their measurements through a chemical modulation technique similar to that described in Tan et al. (2019). This should be addressed, as a significant interference would suggest that the model overestimation of OH could be more significant.

Reply

Thanks for your suggestions, the pre-injector system really did not be applied in this campaign, and it would introduce uncertainty into the OH measurement. However, it is believed that the interference in OH measurement in this campaign was negligible by analyzing the

PKU-LIF system and the environmental conditions during the campaign.

PKU-LIF system has been used to measure HOx concentrations since 2014. We used the pre-injector system to quantify the possible interferences for several campaigns, including the campaigns conducted in Wangdu site (Tan et al., 2017), Heshan site (Tan et al., 2019), Huairou site (Tan et al., 2018), Taizhou (Ma et al., 2022, in review, ACPD), and Chengdu site (Yang et al., 2021). No significant internal interference was found in the prior studies, demonstrating the accuracy of the PKU-LIF system has been determined several times.

Moreover, the potential interference may exist when the sampled air contained alkenes, ozone, and BVOCs (Mao et al., 2012; Fuchs et al., 2016; Novelli et al., 2014), indicating the environmental conditions, especially O_3, alkenes and isoprene, are important to the OH interferences. To further explore the potential interference in this campaign, we take Wangdu campaign as an example to compare the major environmental conditions between the prior campaigns and Shenzhen campaign here. During the Wangdu campaign, the chemical modulation tests were conducted on 29 June, 30 June, 02 July, and 05 July 2014, respectively (Tan et al., 2017). The daily mean O_3, alkenes (ethene, butadiene and other anthropogenic dienes, internal alkenes and terminal alkenes) and isoprene concentrations during the daytime on 29 June were 94.1, 3.8, 1.9 ppb, those on 30 June were 92.2, 2.7, and 1.9 ppb, those on 02 July were 52.9, 1.5, and 0.5 ppb, and those on 05 July were 68.5, 2.4, and 0.9 ppb. The O_3, alkenes and isoprene concentrations on 29 June were highest among those on 29 June, 30 June, 02 July and 05 July, and thus the potential interference on 29 June can be considered the highest among the four days. The results indicated that the potential interference during the daytime in Wangdu was negligible.

Here, we also showed the major parameters related to OH interference in Shenzhen in Table S2 in the Supplementary Information. The daily mean O_3 and isoprene concentrations during the daytime in Shenzhen were within 8.6-91.7 ppb and 0.1-1.0 ppb, which were both lower than those on 29 June in Wangdu. In terms of the alkenes, only 10,16-17 October 2018 in Shenzhen campaign were higher than that observed on 29 June in Wangdu, but the O_3 concentrations on the three days in Shenzhen were only 21.9, 13.9, and 8.6 ppb, and the isoprene concentrations on the three days in Shenzhen were only 0.3, 0.2, and 0.1 ppb, respectively. Overall, the environmental condition in Shenzhen was less conducive to generating potential OH interference than that in Wangdu. Therefore, it is not expected that OH measurement in this campaign was affected by the internal interference.

We have added the description of interval interference in Section 2.2 and the Supplementary Information.

Table S2: The daily mean O_3, alkenes (ethene, butadiene and other anthropogenic dienes, internal alkenes and terminal alkenes) and isoprene concentrations during the daytime (08:00-17:00) in the STORM campaign in this study.

Date / Species	10-05	10-06	10-07	10-08	10-09	10-10	10-11	10-12	10-13	10-14	10-15	10-16
O_3 (ppb)	81.4	83.8	91.7	86.7	48.1	21.9	30.2	42.6	46.8	38.7	40.2	13.9
Alkenes (ppb)	1.4	1.8	3.6	2.3	3.2	5.4	2.9	2.4	2.6	1.4	1.6	4.9
Isoprene (ppb)	0.4	0.4	0.4	0.5	0.4	0.3	0.1	0.3	0.4	0.4	0.6	0.2

Date / Species	10-17	10-18	10-19	10-20	10-21	10-22	10-23	10-24	10-25	10-26	10-27	10-28
O_3 (ppb)	8.6	16.2	39.4	45.8	47.2	25.2	40.9	36.5	55.2	56.5	60.9	60.8
Alkenes (ppb)	4.7	3.2	2.1	1.3	1.2	2.5	2.9	2.7	1.2	3.4	1.7	1.7
Isoprene (ppb)	0.1	0.1	0.5	0.3	0.8	0.8	0.4	0.3	0.5	1.0	0.6	0.8

Revision

(1) Section 2.2:

Additionally, prior studies reported that OH measurement might be affected by the potential interference, when the sampled air contained ozone, alkenes and BVOCs (Mao et al., 2012; Fuchs et al., 2016; Novelli et al., 2014), indicating the environmental conditions are important to the production of interference. The pre-injector is usually used to test the potential OH interference, and has been applied to our PKU-LIF system to quantify the possible interferences for several campaigns, including the campaigns conducted in Wangdu, Heshan, Huairou, Taizhou and Chengdu sites (Tan et al., 2017; Tan et al., 2019; Tan et al., 2018; Yang et al., 2021). No significant internal interference was found in the prior studies, demonstrating the accuracy of the PKU-LIF system has been determined for several times. Moreover, to further explore the potential interference in this campaign, we compared the major environmental conditions, especially O_3, alkenes and isoprene, between Shenzhen and Wangdu sites, as shown in the Supplementary Information. The environmental condition in Shenzhen was less conducive to generating interference than that in Wangdu, and the details were presented in the Supplementary Information. Therefore, it is not expected that the OH measurements in this campaign were affected by the internal interference.

(2) The detailed information on potential OH interference was added in the Supplementary Information:

We compared the environmental conditions in Shenzhen and Wangdu sites. The chemical modulation tests, which was applied to test the potential OH interference, were conducted on 29 June, 30 June, 02 July and 05 July 2014 in Wangdu (Tan et al., 2017). During the campaign in Wangdu, the daily mean O_3, alkenes (ethene, butadiene and other anthropogenic dienes, internal alkenes and terminal alkenes) and isoprene concentrations during the daytime on 29 June were 94.1, 3.8, 1.9 ppb, those on 30 June were 92.2, 2.7, and 1.9 ppb, those on 02 July were 52.9, 1.5, and 0.5 ppb, and those on 05 July were 68.5, 2.4, and 0.9 ppb, respectively. The O_3, alkenes and isoprene concentrations on 29 June were the highest among those on 29 June, 30 June, 02 July and 05 July, and thus the potential interference on 29 June can be considered the highest among the four days. The chemical modulation results indicated that the potential interference during the daytime in Wangdu was negligible (Tan et al., 2017).

As shown in Table S2, the O_3, alkenes and isoprene concentrations in Shenzhen were within 8.6-91.7 ppb, 1.2-5.4 ppb, and 0.1-1.0 ppb, respectively. The O_3 concentrations in Shenzhen (8.6-91.7 ppb) were lower than those on 29 June (94.1 ppb) and 30 June (92.2 ppb) in Wangdu. Similarly, the isoprene concentrations in Shenzhen (0.1-1.0 ppb) were also lower than those on

29 June (1.9 ppb) and 30 June (1.9 ppb) in Wangdu. In terms of the alkenes, only the concentrations on 10, 16-17 October 2018 (4.7-5.4 ppb) in Shenzhen were higher than that observed on 29 June (3.8 ppb) in Wangdu, but the O_3 concentrations on the three days in Shenzhen were only 21.9, 13.9, and 8.6 ppb, and the isoprene concentrations on the three days in Shenzhen were only 0.3, 0.2, and 0.1 ppb, respectively.

Overall, the environmental condition in Shenzhen was less conducive to generating potential OH interference than that in Wangdu. Therefore, it is not expected that OH measurement in this campaign was affected by the internal interference.

4. I assume that the higher NO flow that was used in the HO_2 measurements was required to increase the signal to allow for adjusting the laser wavelength given the failure of the reference cell. Were these measurements included in the data? While the authors claim that the NO concentrations were still low enough to minimize RO_2 conversion to OH, did the authors perform calibrations of some RO_2 conversion efficiencies to confirm this? What HO_2 to OH conversion efficiencies did these two NO flows correspond to? Providing more details on the potential for RO_2 interferences with the HO_2 measurements would improve the reader's confidence in the measurements.

Reply

Thanks for your helpful suggestions. We have rechecked all the data and made corrections in the revised manuscript.

Revision:

(1) Section 2.2:

In this campaign, NO mixing ratios were switched between 25 ppm (low NO mode) and 50 ppm (high NO mode). We calculated the HO_2 conversion rates under the two different NO concentrations by calibrating the PKU-LIF system. HO_2 conversion rates in low NO mode ranged within 80%-95%, while those in high NO mode were over 100%, demonstrating that the HO_2 measurement was affected by RO_2 radicals. Prior studies have reported the relative detection sensitivities (α_{RO_2}) for the major RO_2 species, mainly from alkenes, isoprene and aromatics, when the HO_2 conversion rate was over 100% (Fuchs et al., 2011; Lu et al., 2012; Lu et al., 2013). Therefore, only the HO_2 observations in high NO mode were chosen and they were denoted as $[HO_2^*]$, which was the sum of the true HO_2 concentration and a systematic bias from the mixture of RO_2 species *i* which were detected with different relative sensitivities $\alpha^i_{RO_2}$, as shown in Eq. (1) (Lu et al., 2012). The true HO_2 concentration was difficult to calculated due to the RO_2 concentration measurements and their speciation were not available. Herein, we simulated the HO_2 and HO_2^* concentrations by the model. The interference from RO_2 was estimated to be the difference between the HO_2 and HO_2^* concentrations.

$$[HO_2^*] = [HO_2] + \sum(\alpha^i_{RO_2} \times [RO_2]_i) \quad (1)$$

(2) The figures and descriptions of HO_2 concentration were revised in Section 3.2:

The diurnal maximum of the observed HO_2^*, the modeled HO_2^* and the modeled HO_2 concentrations were 4.2×10^8 cm^{-3}, 6.1×10^8 cm^{-3}, and 4.4×10^8 cm^{-3}, respectively. The difference between the modeled HO_2^* and HO_2 concentrations can be considered a modeled HO_2 interference from RO_2 (Lu et al., 2012). The RO_2 interference was small in the morning, while it became larger in the afternoon. It ranged within 23%-28% during the daytime (08:00-17:00), which was comparable with those in the Backgarden and Yufa sites in China, Borneo rainforest in Malaysia (OP3 campaign, aircraft), and UK (RONOCO campaign, aircraft) (Lu et al., 2012; Lu et al., 2013; Jones et al., 2011; Stone et al., 2014). The observed HO_2^* was overestimated by the model, indicating the HO_2 heterogeneous uptake might have a significant impact during this campaign. The diurnal maximum of HO_2^* concentration observed in Shenzhen was much lower than those observed in the Yufa and Backgarden sites (Hofzumahaus et al., 2009; Lu et al., 2012; Lu et al., 2013).

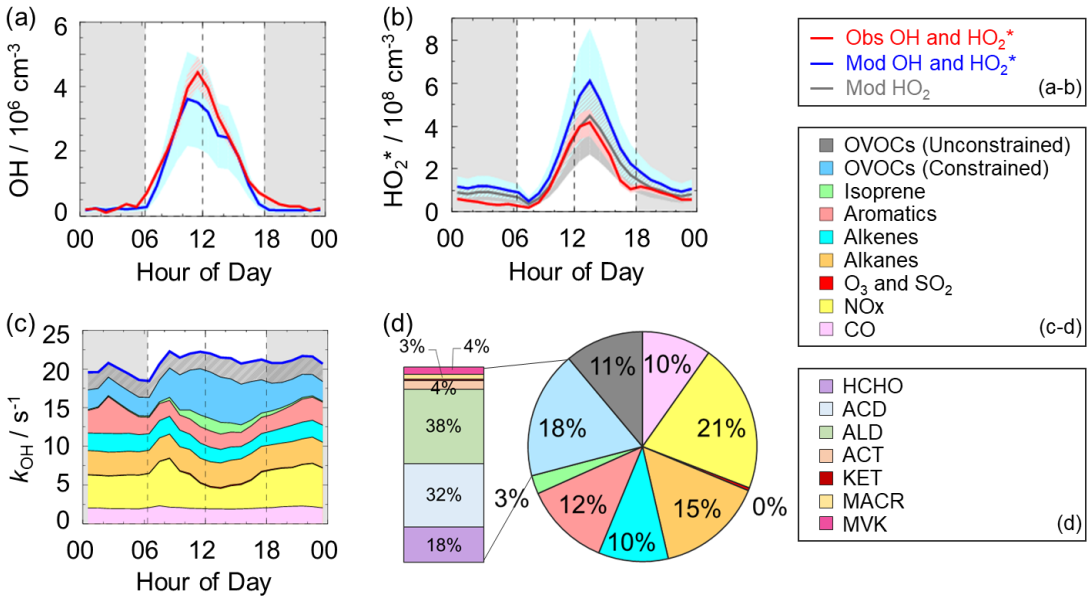

Figure 3: (a-b) The diurnal profiles of the observed and modeled OH, HO_2^* and HO_2 concentrations. (c) The diurnal profiles of the modeled k_{OH}. (d) The composition of the modeled k_{OH}. The red areas in (a-b) denote 1-σ uncertainties of the observed OH and HO_2^* concentrations. The blue areas in (a-b) denote 1-σ uncertainties of the modeled OH and HO_2^* concentrations, and the grey area in (b) denotes 1-σ uncertainties of the modeled HO_2 concentrations. The grey areas in (a-c) denote nighttime. ACD denotes acetaldehydes. ALD denotes the C3 and higher aldehydes. ACT and KET denote acetone and ketones. MACR and MVK denote methacrolein and methyl vinyl ketone.

(3) The timeseries of HO_2 concentrations were revised in Figure S1:

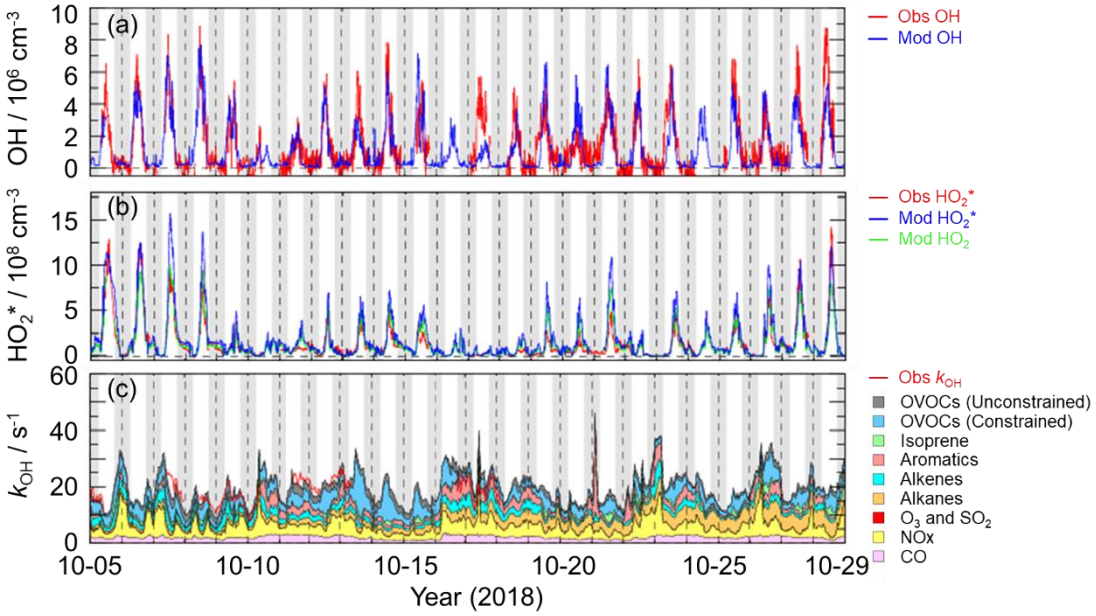

Figure S1: Timeseries of the OH, HO_2^*, HO_2 concentrations and k_{OH} in this study. The grey areas denote nighttime.

(4) The observed HO_2 concentrations can influence the OH experimental budget, so the description in Section 4.1 was revised:

It is noted that the OH production rate was overestimated because we used HO_2^* concentrations instead of HO_2 concentrations here. Thus, the missing OH source was the lower limit here, demonstrating more unknown OH sources need to be further explored.

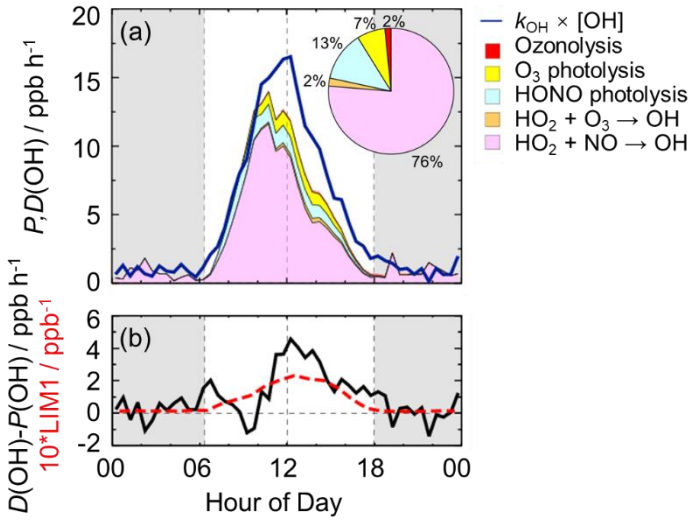

Figure 4: (a) The diurnal profiles of OH production and destruction rates and the proportions of different known sources in the calculated production rate during the daytime. The blue line denotes the OH destruction rate, and the colored areas denote the calculated OH production rates from the known sources. (b) The missing OH source which was the discrepancy between the OH destruction and production rates, and the OH production rate which was ten times the production rate derived from LIM1 mechanism. The grey areas denote nighttime.

(5) The NO dependence of HOx radicals in Fig. 5 was revised:

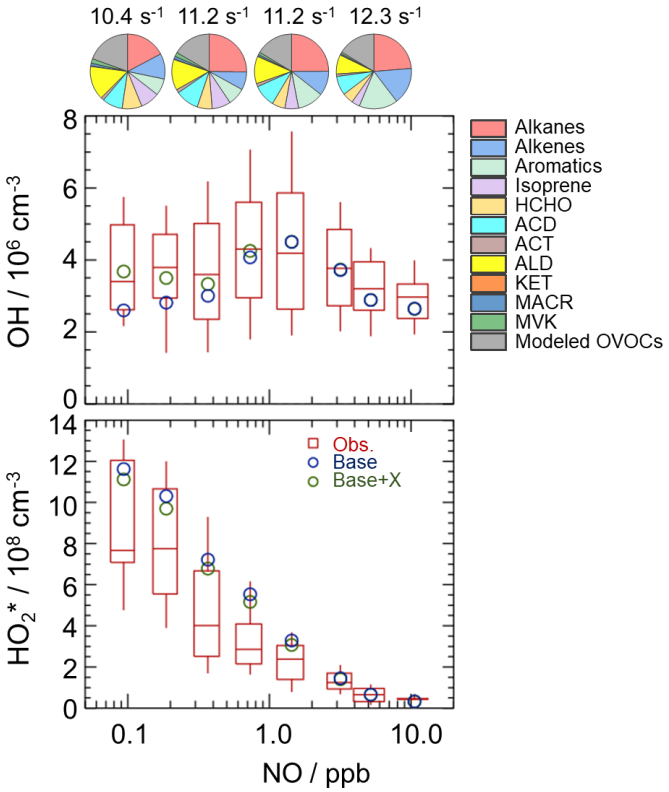

Figure 5: NO dependence of OH and HO_2^* radicals. The red box-whisker plots give the 10%, 25%, median, 75%, and 90% of the HOx observations. The blue circles show the median values of the HOx simulations by the base model, and the green circles show the HOx simulations by the model with X mechanism. Total VOCs reactivity and their organic speciation are presented by pie charts at the different NO intervals at the top. Only daytime values and NO concentration above the detection limit of the instrument were chosen. ACD and ACT denote acetaldehyde and acetone, respectively. ALD denotes the C3 and higher aldehydes. KET denotes ketones. MACR and MVK, which are both the isoprene oxidation products, denote methacrolein and methyl vinyl ketone, respectively.

5. The authors should clarify that the rate of ozone production shown in equation 2 (line 322) represents the gross instantaneous rate of ozone production rather than the net rate of ozone production, as it does not take into account any NO_2 formed that does not lead to O_3 production through the formation of HNO_3 from the OH + NO_2 reaction. In contrast Tan et al. (2017) appear to use the net rate of ozone production in their analysis of the chemistry at the Wangdu site. As a result, the comparison of the rate of ozone production between the sites shown in Figure 7c may not be an appropriate comparison. This should be clarified.

Reply

Thanks for your helpful suggestions. We calculated the net rate of ozone production and added the NO dependence of $P(O_3)$, AOC and the ratio of $P(O_3)$ to AOC in Fig. 7 (b-d).

Revision

(1) Section 4.4:

As the indictor for secondary pollution, net O_3 production rate, $P(O_3)$, can be calculated from

the O_3 formation rate ($F(O_3)$) and O_3 loss rate ($L(O_3)$), as shown in Eq. (3-5) (Tan et al., 2017). The diurnal profiles of the speciation $F(O_3)$ and $L(O_3)$ were shown in Fig. S5 in the Supplementary Information. The diurnal maxima of the modeled $F(O_3)$ and $L(O_3)$ were 18.9 ppb h^{-1} and 2.8 ppb h^{-1}, with the maximum $P(O_3)$ of 16.1 ppb h^{-1} at 11:00. The modeled $P(O_3)$ was comparable to that in Wangdu site in summer and much higher than that in Beijing in winter (Tan et al., 2018; Tan et al., 2017).

$$F(O_3) = k_{HO_2+NO}[HO_2][NO] + \sum_i k_{RO_2i+NO}[RO_2]_i[NO] \quad (3)$$

$$L(O_3) = \theta j(O^1D)[O_3] + k_{O_3+OH}[O_3][OH] + k_{O_3+HO_2}[O_3][HO_2] + (\sum(k^i_{alkenes+O_3}[alkenes^i]))[O_3] \quad (4)$$

$$P(O_3) = F(O_3) - L(O_3) \quad (5)$$

where θ is the fraction of O^1D from ozone photolysis that reacts with water vapor.

Herein, we presented the NO dependence of $P(O_3)$, AOC_{VOCs}, and ratio of $P(O_3)$ to AOC_{VOCs} in Fig. 7 (b-d), in which AOC_{VOCs} denotes the atmospheric oxidation capacity only from the VOCs oxidation. An upward trend $P(O_3)$ was presented with the increase of NO concentration when NO concentration was below 1 ppb, while a downward trend was shown with the increase of NO concentration when NO concentration was above 1 ppb. In terms of the NO dependence of AOC_{VOCs}, no significant variation was found, indicating VOCs oxidation was weakly impacted by NO concentrations in this campaign. Since AOC_{VOCs} can represent the VOCs oxidant rate, and thus the ratio of $P(O_3)$ to AOC_{VOCs} can reflect the yield of ozone production from VOCs oxidation. Similar to $P(O_3)$, the ratio increased with the increase of NO concentration when NO concentration was below 1 ppb. When NO concentration was above 1 ppb, the ratio decreased with the increase of NO concentration because NO_2 became the sink of OH radicals gradually. The maximum of the ratios existed when NO concentration was approximately 1 ppb, with a median of about 2, indicating the yield of ozone production from VOCs oxidation was about 2 in this study.

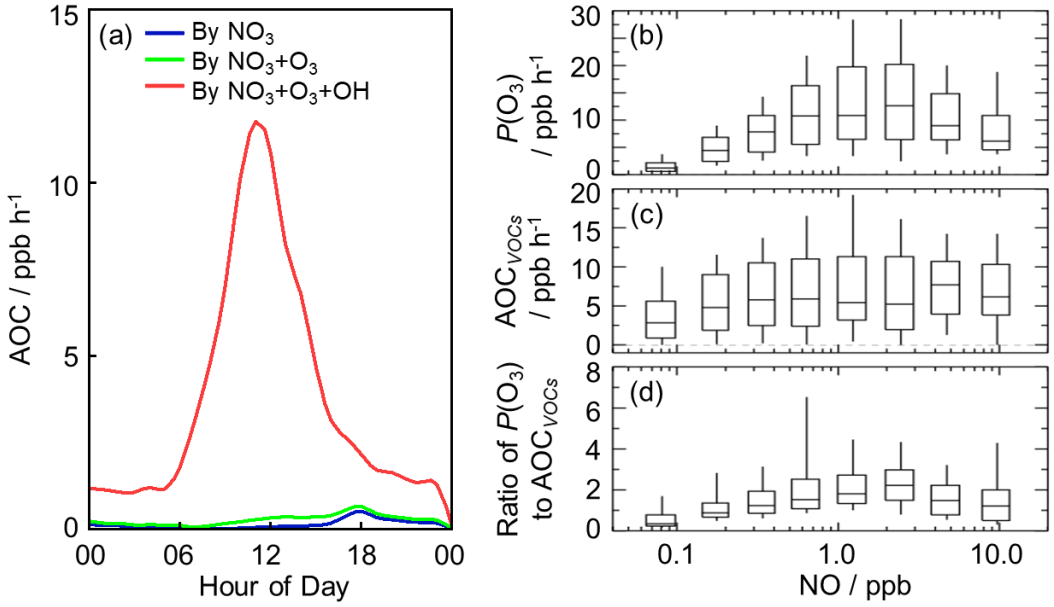

Figure 7: (a) The diurnal profiles of AOC in this campaign. (b) NO dependence of $P(O_3)$ during the daytime. (c) NO dependence

of AOC_{VOCs} during the daytime, and AOC_{VOCs} denotes the atmospheric oxidation capacity only from the VOCs oxidation. (d) NO dependence of the ratio of $P(O_3)$ to AOC_{VOCs} during the daytime. The box-whisker plots in (b-d) give the 10%, 25%, median, 75%, and 90% of $P(O_3)$, AOC and the ratio of $P(O_3)$ to AOC, respectively.

(2) The diurnal profiles of $P(O_3)$, $F(O_3)$, and $L(O_3)$ were added in Figure S5 in the Supplementary Information:

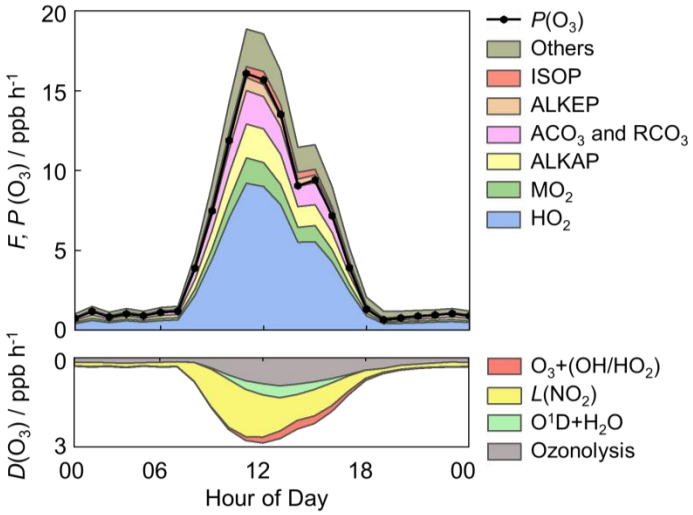

Figure S5: The diurnal profiles of $P(O_3)$, $F(O_3)$, and $L(O_3)$ in this campaign. The colored areas denote the speciation of $F(O_3)$ and $L(O_3)$ in the upper panel and lower panel, respectively. The black line denotes the $P(O_3)$, which is the discrepancy between $F(O_3)$ and $L(O_3)$. MO_2 denotes the methyl peroxy radicals. ALKAP, ALKEP and ISOP denote the RO_2 radicals derived from alkanes, alkenes and isoprene, respectively. ACO_3 denotes the acetyl peroxy radicals, and RCO_3 denotes the higher saturated acyl peroxy radicals.

References

Fuchs, H., Bohn, B., Hofzumahaus, A., Holland, F., Lu, K. D., Nehr, S., Rohrer, F., and Wahner, A.: Detection of HO2 by laser-induced fluorescence: calibration and interferences from RO2 radicals, Atmospheric Measurement Techniques, 4, 1209-1225, 10.5194/amt-4-1209-2011, 2011.

Fuchs, H., Tan, Z., Hofzumahaus, A., Broch, S., Dorn, H.-P., Holland, F., Kuenstler, C., Gomm, S., Rohrer, F., Schrade, S., Tillmann, R., and Wahner, A.: Investigation of potential interferences in the detection of atmospheric ROx radicals by laser-induced fluorescence under dark conditions, Atmospheric Measurement Techniques, 9, 1431-1447, 10.5194/amt-9-1431-2016, 2016.

Hofzumahaus, A., Rohrer, F., Lu, K., Bohn, B., Brauers, T., Chang, C.-C., Fuchs, H., Holland, F., Kita, K., Kondo, Y., Li, X., Lou, S., Shao, M., Zeng, L., Wahner, A., and Zhang, Y.: Amplified Trace Gas Removal in the Troposphere, Science, 324, 1702-1704, 10.1126/science.1164566, 2009.

Jones, C. E., Hopkins, J. R., and Lewis, A. C.: In situ measurements of isoprene and monoterpenes within a south-east Asian tropical rainforest, Atmospheric Chemistry and Physics, 11, 6971-6984, 10.5194/acp-11-6971-2011, 2011.

Lu, K. D., Hofzumahaus, A., Holland, F., Bohn, B., Brauers, T., Fuchs, H., Hu, M., Haeseler, R., Kita, K., Kondo, Y., Li, X., Lou, S. R., Oebel, A., Shao, M., Zeng, L. M., Wahner, A., Zhu, T., Zhang, Y. H., and Rohrer, F.: Missing OH source in a suburban environment near Beijing: observed and modelled OH and HO2 concentrations in summer 2006, Atmospheric Chemistry and Physics, 13, 1057-1080,

10.5194/acp-13-1057-2013, 2013.
Lu, K. D., Rohrer, F., Holland, F., Fuchs, H., Bohn, B., Brauers, T., Chang, C. C., Haeseler, R., Hu, M., Kita, K., Kondo, Y., Li, X., Lou, S. R., Nehr, S., Shao, M., Zeng, L. M., Wahner, A., Zhang, Y. H., and Hofzumahaus, A.: Observation and modelling of OH and HO2 concentrations in the Pearl River Delta 2006: a missing OH source in a VOC rich atmosphere, Atmospheric Chemistry and Physics, 12, 1541-1569, 10.5194/acp-12-1541-2012, 2012.
Mao, J., Ren, X., Zhang, L., Van Duin, D. M., Cohen, R. C., Park, J. H., Goldstein, A. H., Paulot, F., Beaver, M. R., Crounse, J. D., Wennberg, P. O., DiGangi, J. P., Henry, S. B., Keutsch, F. N., Park, C., Schade, G. W., Wolfe, G. M., Thornton, J. A., and Brune, W. H.: Insights into hydroxyl measurements and atmospheric oxidation in a California forest, Atmospheric Chemistry and Physics, 12, 8009-8020, 10.5194/acp-12-8009-2012, 2012.
Novelli, A., Hens, K., Ernest, C. T., Kubistin, D., Regelin, E., Elste, T., Plass-Duelmer, C., Martinez, M., Lelieveld, J., and Harder, H.: Characterisation of an inlet pre-injector laser-induced fluorescence instrument for the measurement of atmospheric hydroxyl radicals, Atmospheric Measurement Techniques, 7, 3413-3430, 10.5194/amt-7-3413-2014, 2014.
Stone, D., Evans, M. J., Walker, H., Ingham, T., Vaughan, S., Ouyang, B., Kennedy, O. J., McLeod, M. W., Jones, R. L., Hopkins, J., Punjabi, S., Lidster, R., Hamilton, J. F., Lee, J. D., Lewis, A. C., Carpenter, L. J., Forster, G., Oram, D. E., Reeves, C. E., Bauguitte, S., Morgan, W., Coe, H., Aruffo, E., Dari-Salisburgo, C., Giammaria, F., Di Carlo, P., and Heard, D. E.: Radical chemistry at night: comparisons between observed and modelled HOx, NO3 and N2O5 during the RONOCO project, Atmospheric Chemistry and Physics, 14, 1299-1321, 10.5194/acp-14-1299-2014, 2014.
Tan, Z., Lu, K., Hofzumahaus, A., Fuchs, H., Bohn, B., Holland, F., Liu, Y., Rohrer, F., Shao, M., Sun, K., Wu, Y., Zeng, L., Zhang, Y., Zou, Q., Kiendler-Scharr, A., Wahner, A., and Zhang, Y.: Experimental budgets of OH, HO2, and RO2 radicals and implications for ozone formation in the Pearl River Delta in China 2014, Atmospheric Chemistry and Physics, 19, 7129-7150, 10.5194/acp-19-7129-2019, 2019.
Tan, Z., Fuchs, H., Lu, K., Hofzumahaus, A., Bohn, B., Broch, S., Dong, H., Gomm, S., Haeseler, R., He, L., Holland, F., Li, X., Liu, Y., Lu, S., Rohrer, F., Shao, M., Wang, B., Wang, M., Wu, Y., Zeng, L., Zhang, Y., Wahner, A., and Zhang, Y.: Radical chemistry at a rural site (Wangdu) in the North China Plain: observation and model calculations of OH, HO2 and RO2 radicals, Atmospheric Chemistry and Physics, 17, 663-690, 10.5194/acp-17-663-2017, 2017.
Tan, Z., Rohrer, F., Lu, K., Ma, X., Bohn, B., Broch, S., Dong, H., Fuchs, H., Gkatzelis, G. I., Hofzumahaus, A., Holland, F., Li, X., Liu, Y., Liu, Y., Novelli, A., Shao, M., Wang, H., Wu, Y., Zeng, L., Hu, M., Kiendler-Scharr, A., Wahner, A., and Zhang, Y.: Wintertime photochemistry in Beijing: observations of ROx radical concentrations in the North China Plain during the BEST-ONE campaign, Atmospheric Chemistry and Physics, 18, 12391-12411, 10.5194/acp-18-12391-2018, 2018.
Yang, X., Lu, K., Ma, X., Liu, Y., Wang, H., Hu, R., Li, X., Lou, S., Chen, S., Dong, H., Wang, F., Wang, Y., Zhang, G., Li, S., Yang, S., Yang, Y., Kuang, C., Tan, Z., Chen, X., Qiu, P., Zeng, L., Xie, P., and Zhang, Y.: Observations and modeling of OH and HO2 radicals in Chengdu, China in summer 2019, The Science of the total environment, 772, 144829-144829, 10.1016/j.scitotenv.2020.144829, 2021.